Modelling an integrated blockchain-based energy optimization platform with bilateral trading for microgrid communities

MSc Thesis Energy Science

Gijs van Leeuwen

Student number: 4048873

First supervisor: Dr. Tarek AlSkaif

Second supervisor: Prof. Dr. Madeleine Gibescu

July 2019

Abstract

The increase in residential solar energy and other Distributed Energy Resources (DER) calls for novel energy management solutions in the low-voltage (LV) distribution grid. Such solutions may come in the form of digital Peer-to-Peer (P2P) energy trading platforms or the emergence of energy communities where households share electricity between them through a microgrid in an optimized manner. In such networks it is common to have a third party as a central coordinator, in which case issues of privacy, security and independence arise. A solution may be found in blockchain and smart contract technology which allows for decentralized and secure coordination of self-interested and independent actors. In this thesis, an integrated blockchain-based energy management platform is modelled that will optimize energy flows in a microgrid whilst implementing a bilateral trading mechanism. physical constraints in the microgrid are respected by formulating an Optimal Power Flow (OPF) problem, which is combined with a bilateral trading mechanism in a single optimization problem. It is one of the first times such an integrated, combined optimization problem has been proposed. The Alternating Direction Method of Multipliers (ADMM) is used to decompose the problem to allow for distributed optimization and a smart contract is used to function as a virtual aggregator. The smart contract fulfills several functions, including distribution of data to all participants and executing part of the ADMM algorithm. The model is run using real data from a prosumer community in Amsterdam and several scenarios are tested to evaluate the impact of combining physical constraints and trading on performance of the algorithm, social welfare of the community and scheduling of energy flows and trading scheme. It is found that the combination of trading and physical constraints in a single optimization problem may mitigate inequality between households within the community. Furthermore, total costs of the whole community are reduced by 22% as compared to a baseline scenario, and total grid energy consumption is reduced by 30%. Total social welfare is found to be highest when optimizing energy flows based on physical constraints without using a trading mechanism, however such a platform is only viable when all costs are equally shared between all households. The combined scenario is found to give only a slightly lower total social welfare than the trade-only scenario, with the added benefit that the inclusion of grid constraints may dampen the market power of prosumers in the community, decreasing inequality between households.

Contents

List of Figures

List of Tables

Nomenclature

Abbreviations

AC	Alternating Current
ADMM	Alternating Direction Method of Multipliers
DER	Distributed Energy Resources
EV	Electric Vehicle
FiT	Feed-in-Tariffs
HEMS	Home Energy Management System
ICT	Information and Communication Technology
LV	Low Voltage
OPF	Optimal Power Flow
P2P	Peer-to-Peer
PV	Photovoltaics
SOC	Second Order Cone

Parameters

$\boldsymbol{\Gamma}^{\mathrm{b,rel}}$	Relative willingness of households to buy
$\boldsymbol{\Gamma}^{\mathrm{b,rel}}$	Relative willingness of households to sell
$\boldsymbol{\sigma}$	The smart contract
$\boldsymbol{P}^{\mathrm{c}}$	Fixed real power load matrix
$\boldsymbol{P}^{\mathrm{net}}$	Net electricity budget matrix
$\boldsymbol{P}^{\mathrm{pv}}$	PV generation matrix
η_{in}^{b}	Battery charging efficiency
η_{out}^{b}	Battery discharging efficiency
Γ	Bilateral trading coefficient matrix
κ_t	Costs of withdrawing from the external grid per kWh
λ	Blockchain network adress
ω	Binary EV scheduling parameter
ϕ	Penalty parameter for trading mechanism
ρ	Penalty parameter for grid constraints
E_i^{ev}	Average daily EV charging demand
p^{c}	Fixed real power load
p^{pv}	PV power generation
q^{c}	Fixed reactive power load
r	Resistance
T	Number of timesteps

x	Reactance
Sets	
$\mathcal{A}$	Set of assets
$\mathcal{M}$	Set of trade partners
$\mathcal{N}$	Set of nodes
θ	Set of constructor variables
x_l	Set of local private variables
x_u	Set of local coupling variables
z_g	Set of global variables
Variables	
$\boldsymbol{D}$	Trading quantity matrix
ν	Squared voltage
ψ	Squared current
ξ	Price of trading and dual variable for trading mechanism
C^g	Total costs of external grid withdrawal
e^{b}	Battery state of charge
k_g	Number of local variable components corresponding to global variable
P	Real power flow
p	Net real power
p^g	Real power withdrawn from the external grid
p^{bc}	Battery charging power
p^{bd}	Battery discharging power
p^{b}	Net battery power generation
p^{ev}	Real power consumption of EV
Q	Reactive power flow
q	Net reactive power
q^g	Reactive power generation
r_{grid}	Primal residual for grid constraints
r_{trade}	Primal residual for trading mechanism
S	Complex power flow
s_{grid}	Dual residual for grid constraints
s_{trade}	Dual residual for trading mechanism
y	Dual variable for grid constraints

1 Introduction

1.1 Background

Several concurrent developments are profoundly transforming the energy system as we know it today. The main driver for this originates in 2015, when 195 countries committed themselves to keeping global temperature rise in 2050 below 2°C as compared to pre-industrial levels in order to mitigate harmful climate change effects. In order to attain this goal, it is necessary to greatly reduce emissions of greenhouse gases, the foremost among them being CO_2 [1]. The largest source of CO_2 emissions is the burning of fossil fuels such as coal, natural gas and oil, and it is these fuels upon which the entire energy system is based. Fossil fuels are used both as a primary source of fuel, for example in internal combustion engines, but are also used to generate electricity. In order to reduce CO_2 emissions to the extent that is needed, alternative, clean sources of energy must be found and realized [2]. More and more policy options are becoming available for achieving these goals. These policies may come in the form of CO_2 pricing [3], subsidizing of renewables [4] or the institution of Feed-in-Tariffs (FiT) [5] to allow owners of residential Photovoltaics (PV) systems to sell their energy surplus back to the grid. Currently the most promising technologies for generating renewable energy on a large scale are wind energy and solar PV energy [6] [2].

There are several fundamental differences between fossil fuel technologies and renewable energy technologies. First of all, fossil fuels are very flexible. A power generation plant running on natural gas may be turned on and off at any time, and the amount of power generated may be increased or decreased at will. Additionally, transporting and storing fossil fuels is easy and straightforward given their chemical substantiality. Large amounts of fuel may be amassed in one place for electricity generation, allowing for high efficiency [2]. Since all of human society is dependent on fossil fuel generated energy, this flexibility is taken for granted. for wind and solar energy, the situation is different. The quantity and timing of energy generated are dependent on environmental conditions which are outside of human control. Electricity can no longer be generated on demand at any time, in any quantity. Furthermore, the energy density of wind and sunlight is relatively low [2]. This means that, whereas fossil fuels can be burned in large quantities to generate large amounts of power in a single place, renewable energy is generated in a large number of small capacity generator units that are distributed over a wide geographical area. As a consequence, transportation of energy no longer occurs by moving a physical substance but instead by transmitting electricity.

For these reasons, a substantial replacement of fossil fuel-based energy with renewable energy will require a fundamental transformation of the whole energy system, in particular the electricity grid. Currently, the vast majority of electricity is generated in several primary power plants, and is subsequently transmitted over high voltage transmission networks to all regions of a country. Then, electricity is distributed through the distribution network towards small consumers such as households. This flow of electricity is a top-down, one-way process. As a larger portion of electricity is generated by renewable means however, this hierarchical network will not be capable of facilitating optimal distribution. The wide geographical distribution of wind and particularly PV means that to an increasing degree, electricity will be generated in areas where the distribution grid is not properly equipped to facilitate this [7]. These locations may include lesser populated areas but also urban environments and privately owned property. On these fringes of the distribution network, it will be required to install much more complex coordination and control systems to enable the bidirectional flow of electricity [8]. These consequences are amplified by the electrification of various technologies that have up to now operated on fossil fuels, e.g. heat pumps and Electric Vehicles (EV). Adoption of these technologies will cause a significant rise in electricity demand, and in the case of EV, the installation of new infrastructure is required in the form of charging stations, causing further strain on the distribution network. Together, these geographically dispersed electricity generating and consuming technologies can be referred to as Distributed Energy Resources (DER).

Whilst these developments pose considerable technical challenges for grid operators, governments and other stakeholders, opportunities may also arise for regular citizens. Already, the increasing adoption of residential solar PV has led to an increase in the number of prosumers in the electricity market [9]. Prosumers are both producers and consumers of electricity, withdrawing electricity from the grid in the conventional manner as well as selling back electricity generated by their local PV systems at times that they do not consume it. In various countries, FiT are in place to facilitate prosumers [5], allowing them to sell PV-generated energy back to the grid for a fixed price. Whilst FiT do provide a solution, it is by no means an optimal one. First of all, several countries including The Netherlands are planning to abolish FiT in the coming years [10]. Secondly, it is more efficient, energetically as well as financially, to optimize local use of energy and minimize interaction with the grid [11]. This can be enabled by the deployment of energy storage

systems, and the use of schedulable electrical appliances or EVs that are configured to operate or charge at times when generation exceeds consumption [12]. Still, there is only so much a single prosumer can do to balance energy management at the household level. A larger degree of efficiency and flexibility may be reached when generation and consumption are balanced between a number of households. Such solutions involving multiple households may be implemented in novel types of consumer-centric electricity markets [13], where prosumers can trade or share energy between them based on their respective consumption and generation patterns. In other sectors, similar developments are already taking place, enabled by digital platform technologies and new economic principles such as the sharing economy [14]. These new types of markets are called Peer-To-Peer (P2P) markets [15]. P2P markets allow agents to conduct trades without involvement of a third party. Information and Communication Technology (ICT) is used to match supply and demand and trades are generally conducted as one-off transactions rather than long-term contracts. Companies such as Uber and AirBnB are examples of this. P2P markets may be designed to prioritize the wellbeing of the participating individuals by providing maximum individual freedom, financial independence and privacy, or alternatively they may focus more on the welfare of the community as whole, where participants may choose to share access to a common resource and aim to achieve a common goal such as total welfare maximization or autonomy [15]. P2P markets are now started to emerge in the energy sector [16]. This can be recognized in the rise of community-based energy collectives [17] [18] [13]. The new P2P market constructs may allow small prosumers to trade energy directly with each other and decrease their dependency on retail markets which are not transparent and more expensive because of energy service company fees [18].

The evolution of the electricity grid into a decentralized, distributed network is enabled by several important advancements in ICT technology. First of all, recent years have seen a large increase in the number of installed smart metering systems in Europe [9]. Smart meters measure electricity consumption and generation and allow bidirectional flow of information between a household and the energy service company [19]. These smart meters generate vast amounts of data as they operate in real time as opposed to traditional metering systems. Analysis of these large amounts of data provide insight into energy consumption and generation patterns and further enable energy management solutions and smart optimization of energy flows [20]. The EU Recommendation 2012/148/EU states that by 2020 a roll out of smart metering systems of at least 80% should be achieved and emphasizes that smart meters should assist the active participation of consumers in the electricity supply market [9] [21]. Expanding on a smart metering system is the home energy management system (HEMS) [22]. A HEMS is a system that is capable of measuring and controlling the operation of all connected electrical assets in a household, including appliances, solar panels, batteries and EVs. A centrally coordinating computer can optimally balance power usage in the household by automatically directing charge and discharge of batteries at appropriate times and scheduling appliances to operate at times over abundant supply. Furthermore, a HEMS may communicate with the external grid and the energy service company to receive information about electricity tariffs and the state of the grid.

Finally, digital platform technologies have shown their disruptive potential in the past few years. Besides transforming the way in which markets function, through these platforms it is now easier than ever for groups of people to organize themselves and exchange goods and information. This may raise issues when the platform being utilized is owned by a third party with its own interests [23]. Personal information that is stored on the platform may be stolen or abused for commercial purposes. Furthermore, the algorithms that run the functionality of the platform are often not transparent for users, and the controlling party may design these algorithms with only their own interests into consideration. Also, such a centralized platform may be vulnerable to cyberattacks and tampering by attackers, since all information is stored in a single location. Recently, the emergence of blockchain technology may provide a solution to these problems [23] [24]. A blockchain is a type of distributed ledger technology that is used to connect a large number of anonymous nodes without the need for a central controlling agent. Blockchain technology utilizes a consensus mechanism to ensure security of the network and allows participants to store and share data in a secure and verifiable manner, even when the identity and trustworthiness of other peers is unknown. In order for a piece of data to be validated, its source must be verified by other nodes on the network by using cryptographic hashes. Information is stored in sets of data called blocks. A block receives a cryptographic signature which contains information about its contents and is formed when a predefined number of nodes complete a consensus algorithm. Participants can join or leave the blockchain network at any moment without impacting the operation of the system significantly and it is extremely difficult for external attackers to gain control of the blockchain. The clearest application for blockchain has proved to be verification of ownership, as is the case with cryptocurrency [25], but distributed computation between all connected devices is also possible. Extension of a blockchain with smart contract technology expands the utility even further and enables smart

optimization [23] [26].

1.2 Literature Review

Although there is not yet a universal consensus in the scientific community on the terminology used in this field of research, most of the work that shall be considered can be categorised under the term "transactive energy" [27]. Something that all transactive systems have in common is that the system attains global goals through interactive and networked cooperation of independent and self-interested actors. A precursor to transactive energy systems can be recognized in demand response programmes, which mainly provide financial incentives for consumers to withdraw energy from the grid during off-peak hours [28] [29]. Chen and Liu [30] show the evolution from demand response programmes to transactive energy, with the fundamental difference being that transactive systems manage both the demand and the supply of energy, incentivizing both local generation and demand at favourable times. This progression is necessary with the rise of DER and prosumers. Since transactive systems involve interactions between a large number of self-interested actors, the design of transactive systems should align individual behaviour with the goals of the system as a whole [30].

As defined in another study [27], there are three transactive techniques that can be applied to power grids. There is the method of "Distributed, Constrained Economic Power Flow", which has a strong foundation in physics, there are the "Bilateral Trades" which has a foundation in economics, and there is the "Auctions" method that has the middle ground between the two others. Since ultimately both the economic and physical layer are required, the development of practical applications requires alignment of business plans and engineering techniques, which is a considerable challenge. The various layers of a transactive energy system are also emphasised by Zhang et al. [31] who distinguish the four layers of the physical grid, ICT, control and market. The scientific literature concerning the physical, economic and information layers is reviewed. In the information layer, the review is limited to research related to blockchains in the energy sector. Additionally, scientific literature regarding distributed optimization methods shall be reviewed.

In the physical grid, the problem to be solved is to find the optimal electricity flows within the distribution grid while respecting physical constraints relating to power lines and connected assets. A common method of solving this problem is by formulating an Optimal Power Flow (OPF) problem [32]. This is a mathematical optimization problem that finds the optimal configuration of power flows and voltage levels whilst considering losses and balancing constraints to attain a certain optimization objective. The objective is typically to minimize operation costs. OPF problems can be solved for both DC and AC systems and have been in use to solve issues in the main electricity grid and many scientific studies have recently used OPF to find the optimal configuration of power flows in a microgrid [31] [33] [34] [35] [36]. A detailed account on how to apply OPF in a distributed optimization scenario is given by Kraning et al. [37]. Carli & Dotoli [33] use OPF for the energy management of smart homes that have a number of smart, controllable appliances to find the optimal schedule for all of these connected assets. One particularly interesting study conducted by Munsing et al. [35] implements an AC-OPF problem on a blockchain platform for decentralized optimization. Aside from OPF, power flow tracing methods have been used by Di Silvestre et al. [38] to allocate losses in power flow to different agents financially.

The economic layer is where most research has been conducted. In this category both market schemes and prosumer engagement methods shall be considered. Broadly speaking two categories of market structures can be distinguished [18]. On the one hand there is the full P2P market, where trades are conducted bilaterally and there is no centralized supervision. In such a market, all peers operate in a self-interested manner by maximizing their own profit. Maximum independence, freedom and anonymity are guaranteed in a full P2P market [15]. Full P2P markets in the energy sector have been explored in various recent studies [31] [39] [40]. Morstyn et al. [39] designed a scalable economic and financial model for P2P trading with bilateral contract networks. Contracts are made between producers, intermediaries and inflexible consumers. One iconic study from the Brooklyn microgrid [41] has implemented a P2P trading scheme in a real physical microgrid. Supply and demand bids are matched using a conventional merit-order dispatch. The second category of market structures is the energy collective or community based market. In this system, the interest of the group is paramount, and individual agents may sacrifice some of their own profit for the collective social welfare. Moret & Pinson [42] propose a model where energy collectives may decide upon different goals, including total welfare maximization or autonomy from the external grid. They employ a community manager for central coordination and use fairness indicators to ensure equality between all participants. Long et al. [43] study a scenario where energy is shared in a microgrid by using batteries and show benefits for individuals as well as the community as a whole. Tushar et al. [44] take a similar approach using an auction scheme.

Luth et al. [45] conducted a study where market schemes including both individual and community-owned battery storage systems are employed. In these community-based schemes, the electricity price is usually uniform across the community. Recently, a unified prosumer peer-to-peer market model has been formulated by Baroche et al. [46]. This scheme may be operated with both bilateral trades and a centralized pool market, and provides an option for participants to declare preferred trading partners by including a trading penalty.

Although most of the aforementioned studies explore financial benefits for participants, many alternative ways have been suggested to engage prosumer participation. Faber et al. [47] emphasise the usefulness of allowing prosumers to declare trading preferences regarding the source and type of energy that is traded in the market. This is implemented by Sorin et al. [48] who design a full P2P market using the method of Multi-Bilateral Economic Dispatch and include product differentiation and consumer preferences. Gamification-based approaches may also be used to engage prosumers and incentivize participation. Such schemes have been proposed by AlSkaif et al. [12] and Wang et al. [49]. Li et al. [50] employ a Stackelberg game where a credit bank acts as game leader for fast and frequent energy trading in the context of the Industrial Internet Of Things and further incentivize participation by awarding energy coins. In order to effectively incentivize prosumer participation, it is also necessary to have a good insight into their behaviour. Lampropoulos et al. [51] propose a methodology for modelling behaviour of electricity prosumers within the smart grid, to gain insight into the factors that shape residential loads and influence participation.

In the information layer, the application of blockchain technology in the energy sector has been rapidly gaining attention from the scientific community. Blockchain technology is an enabling technology that may improve functionality in many different areas by removing the need for intermediaries. An extensive review was conducted by Andoni et al. [23] who cite a large number of studies and initiatives that have employed blockchain in the energy sector. This includes energy service company operations (e.g. sales, billing etc.), wholesale energy trading and supply and coordination of Internet of Things platforms. In particular blockchain is seen as promising in the area of P2P trading and decentralized energy, since through blockchain a large number of self-interested actors can be connected and coordinated. Thus, by providing anonymity and independence for participants, the use of blockchain may incentivize participation. The overall conclusion in this study is that blockchains may provide clear benefits to energy system operations, markets and consumers. The case study of the Brooklyn microgrid employs a blockchain network to connect participants [41], and shows that a blockchain can be successfully used to implement local electricity markets. Munsing et al. [35] expand on this by employing smart contracts on the blockchain network to enable decentralized optimization of an OPF problem without a central coordinator, as well as for billing using tokens. Other studies that use blockchains and smart contracts for electricity trading include Liu et al. [52] and Li et al. [50]. In the technical domain, Di Silvestre et al. [38] review technical issues related to the use of blockchains in microgrids, and the specific requirements for their setup in this case.

In the domain of distributed optimization algorithms there are several options that may be used to solve an OPF problem or ensure market clearance. Kargarian et al. [34] conducted a review of the suitable for this purpose for six decentralized algorithms, including Analytical Target Cascading (ATC), Alternating Direction Method of Multipliers (ADMM), Proximal Message Passing (PMP), Auxiliary Problem Principle (APP), Optimal Condition Decomposition (OCD) and Consensus + Innovations (C+I). Of these options, ADMM has seen the most extensive application in decentralized energy platforms. Baroche et al. [46] state that ADMM is preferred over C+I for convergence speed and robustness. The ADMM algorithm is well suited to distributed convex optimization and operates by allowing decomposition of a global optimization problem into several sub-problems [53]. The sub-problems are solved in parallel and their solutions are coordinated to come to a solution of the global problem [53]. ADMM has been used by the scientific community to solve optimization problems in both the physical and economic layer. An OPF problem can be decomposed into sub-problems using ADMM, where every sub-problem is related to a small part of the grid. This has been shown in great detail by Kraning et al. [37] who combine ADMM and PMP to optimize power flow in a network including various types of devices, including generators, fixed loads, storage devices and deferrable loads, which are connected by both AD and DC lines. ADMM has been used extensively in other recent studies to decompose OPF problems [33] [35] [54]. Similarly, ADMM can also be utilized to decompose a market clearing optimization problem, where a common approach is to formulate the global optimization problem as a maximization of total social welfare. The problem is decomposed into subproblems that maximize total welfare for every individual agent, and are again coordinated to achieve a global optimum [18] [46] [42].

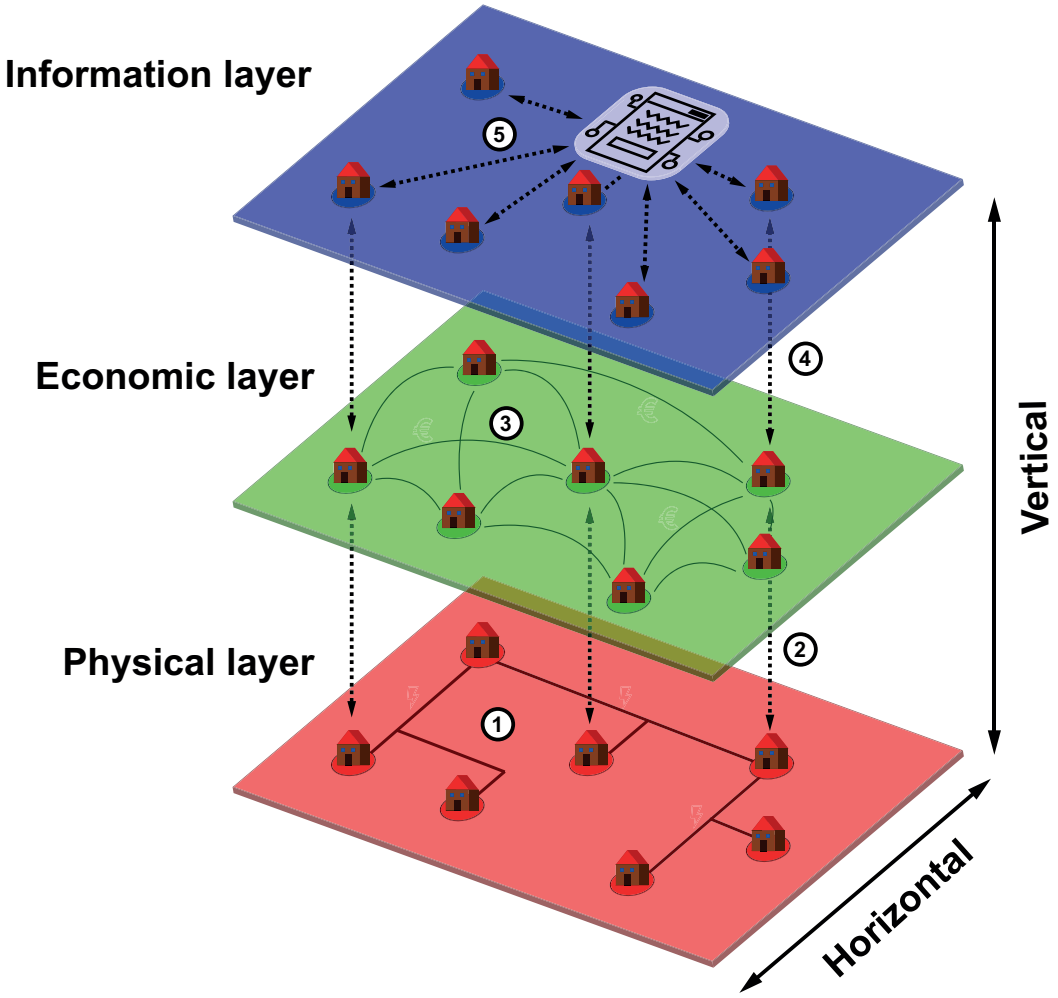

Figure 1: Illustration of the different layers of the proposed model and the interaction between them. 1) In the physical layer, power flows in the horizontal dimension between households through grid connections and is constrained by technical limitations. OPF is used to find the optimal solution. 2) Information is exchanged in the vertical dimension between the economic and the physical layer. This means that households combine information from the both layers to find their optimal scheduling of their DER and trading. 3) In the economic layer, a trading mechanism used to enable monetary compensation for power injections and withdrawals into/from the grid. Money is exchanged horizontally between the households. 4) Information is exchanged between the information layer and the layers below. The households send their locally calculated optimal schemes for the economic and physical layers to the smart contract in 5). The smart contract gathers the optimal solutions from all households and determines how the schemes must be adapted to come to universal agreement. Each household then receives the feedback on how they must adapt their optimal schedule.

1.3 Contributions of this study

The aim of this study is to model an integrated energy management platform that implements solutions in the physical, economic and information layers. The goal of the platform is to optimize the flow of electricity in a distributed manner, in a realistic microgrid configuration which features a number of households with access to a variety of DER. OPF is used in the physical layer to ensure that physical constraints and balancing of power are respected. In the economic layer, a bilateral trading mechanism is implemented to provide personal choice and freedom to the households. In the information layer, the model is implemented on a blockchain network to allow for secure and transparent distributed operation. A smart contract is used to coordinate between the households on the network by acting as a virtual aggregator. Figure 1 shows the structure of the platform. The goal of optimization is to maximize total social welfare of all connected actors. Social welfare is typically represented by financial costs. As such, the optimization objective is to minimize total costs of all households. The ADMM algorithm is used to solve the optimization problem in a distributed manner. The modelled platform is intended to provide a high degree of independence, privacy and transparence by the implementation on the blockchain network, as well as personal choice and freedom through bilateral trading.

Although similar models have been developed before, as has been shown in section 1.2, there are several novel contributions that this study intends to make.

First of all, to the author's best knowledge there have not been any such models proposed that have combined the problems of the technical and economic layers in a single integrated model. In the current proposal, an AC-OPF problem will be formulated and combined with a bilateral trading mechanism in a single optimization problem that respects grid limitations and achieves market clearance by optimally scheduling power flows and the trading scheme. This is one of the first times such an integrated model is proposed. In order to assess the performance of the integrated model, a comprehensive numerical analysis is performed and a number of performance parameters is evaluated.

As a second major contribution, the implementation on the blockchain platform and specifically the role of the smart contract are described in a detailed manner. The smart contract fulfills the role of a virtual aggregator and executes several parts of the ADMM algorithm. It acts as a coordinator that ensures symmetric execution of the algorithm by all actors, and with which all agents on the network must communicate and exchange information. At every stage in the execution of the ADMM algorithm, the flow of information between the smart contract and the agents on the network is described.

Given these contributions, the research questions are formulated as follows:

1. How does the combination of physical grid constraints and trading mechanism in a single optimization problem impact performance of the model?
   (a) How does the combination affect convergence of the ADMM algorithm?
   (b) How does the combination affect social welfare?
   (c) How does the combination affect scheduling of power flows and trading scheme?
2. How can a smart contract fulfill the role of virtual aggregator in the ADMM algorithm?
   (a) What are the different functions the smart contract has to execute in the role of virtual aggregator?
   (b) How is the flow of information between agents on the network and the smart contract?

The paper is structured as follows. The methodology is presented in section 2, where the general layout and setup of the grid and households are presented in subsection 2.1. The centralized formulations of the OPF problem and trading mechanism are given in subsections 2.2 and 2.3 respectively, and the decentralized formulations of both are given in subsection 2.4. The blockchain implementation is detailed in subsection 2.5 and the configuration of the numerical analysis can be found in subsection 2.6. The results are given in section 3, and a discussion of these results is found in section 4. Finally, the thesis is concluded in section 5.

2 Methodology

As a basis for answering the research questions a decentralized blockchain-based P2P trading platform is modelled. The platform is designed to function on a microgrid network that features consumers and prosumers with access to private EV charging stations, solar PV installations and batteries. The platform is intended to function as a day-ahead energy scheduling platform, where energy management is optimized for 24 hours the day ahead. Every prosumer household is considered as a separate node on the network that consumes and/or generates energy, and an AC-OPF problem is formulated to optimize energy flows. Households are able to trade their excess or deficit electricity budget between them by assigning bilateral trading coefficients to different trading partners at different timesteps. This allows for differentiation of energy products or designation of preferred trading partners. The main novelty in the proposed platform is that the technical and the economic optimization problems are combined into one. This optimization problem is formulated in a distributed form using the ADMM algorithm. Finally, the distributed optimization problem is implemented on a private blockchain test network by porting part of the algorithm's functionality to a smart contract that is deployed on the blockchain network. In order to evaluate the impact that inclusion of grid constraints and trading mechanism have on social welfare and power flows, different versions of the platform are tested that include and exclude the grid constraints and the trading mechanism. Furthermore, convergence of the ADMM algorithm is also evaluated under these different scenarios. A comparison is also made with a baseline scenario in which the microgrid is non-existent and there is only interaction between households and the external grid.

2.1 Grid and household setup

The microgrid considered in this study is modelled as a radial Low Voltage (LV) network for a number of timesteps T, indexed by $t = 0, 1, \ldots, T$. It can be represented by a set of nodes $\mathcal{N}$, indexed by $i = 0, 1, \ldots, n$, and connecting lines $\mathcal{L}$. Node 0 is designated as the root node. A node in $\mathcal{N}$ can be either referred to with its index number i or as a neighbouring node of another node j. In this relationship, j is defined as the node that is closer to the root node. As such, j is called the parent node of i, and can be referred to as $\pi(i)$. In similar fashion, node i is called the k-th child node of j, and can be referred to as $\delta_k(j)$. Due to the radial nature of the network, every node will only have one parent node. A node can have multiple children, and the set of children nodes of node j is referred to as $\delta(j)$, indexed by $k = 0, 1, \ldots, c$. For simplicity, every line in $\mathcal{L}$ is designated to have the same index number as the connected child node. In every line i, the complex impedance is denoted as $z_i = r_i + \mathtt{i}x_i$, where r and x are the resistance and reactance in the line. A 4-node illustration can be seen in Figure 2.

All households in $\mathcal{N}$ have a number of assets available to them that influence the flow of power. First of all, all households have access to a one-way connection to the external grid, as FiT are not considered in this study. Power withdrawn from the external grid is designated as $p^{\mathrm{g}}_{i,t}$. The costs of withdrawing power from the grid is represented by κ_t. The costs for each household i in timestep t is given by:

$$C^{\mathrm{g}}_{i,t}(p^{\mathrm{g}}_{i,t}) = p^{\mathrm{g}}_{i,t}\kappa_t, \quad \forall\, i, t. \tag{1}$$

Every household also has a fixed real power load $p^{\mathrm{c}}_{i,t}$ and fixed reactive power load $q^{\mathrm{c}}_{i,t}$ that are uncontrollable. Controllable reactive power generation $q^{\mathrm{g}}_{i,t}$ is assumed to be available to those households that have access to solar PV [55]. The generation of real and reactive power is constrained within upper and lower limits as follows:

$$\underline{p}^{\mathrm{g}}_i \leq p^{\mathrm{g}}_{i,t} \leq \overline{p}^{\mathrm{g}}_i, \quad \forall\, i, t, \tag{2a}$$

$$\underline{q}^{\mathrm{g}}_i \leq q^{\mathrm{g}}_{i,t} \leq \overline{q}^{\mathrm{g}}_i, \quad \forall\, i, t. \tag{2b}$$

Other assets that are available only to some households but not others include solar PV, EV and battery systems. The availability of solar PV yields a fixed, uncontrollable power generation $p^{\mathrm{pv}}_{i,t}$. The availability of EV and battery systems yields additional constraints. An EV is considered to be a shiftable load where both the time and quantity of the charging power $p^{\mathrm{ev}}_{i,t}$ can be controlled. Total daily charge must equal the average daily charging demand of an EV E^{ev}_i, as can be seen in (3). Furthermore, EV charging rate must be within upper and lower charging limits. A binary parameter $\omega_{i,t}$ is used in (4) to indicate the timeslots at which the EV charging can be scheduled.

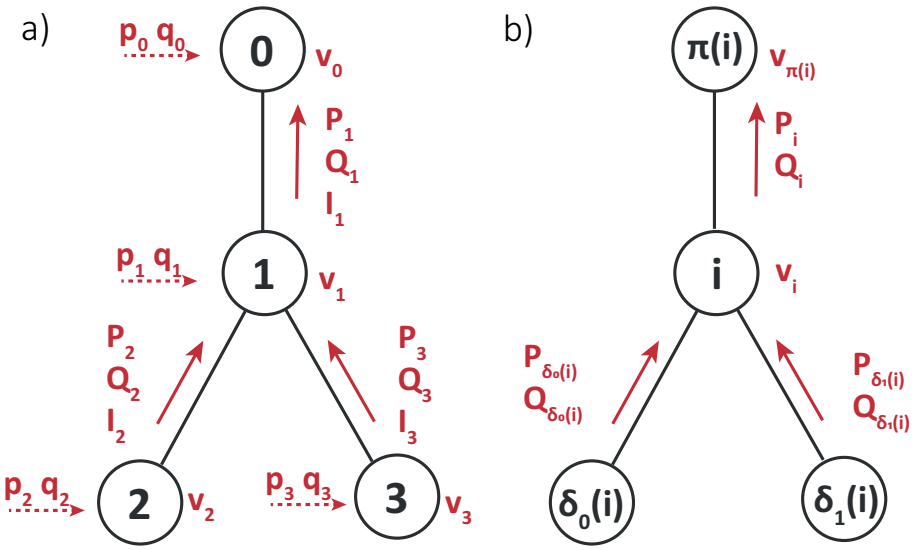

Figure 2: Illustration of the grid setup and power flow dynamics with 4 nodes.

$$\sum_{t=0}^{\mathrm{T}} p_{i,t}^{\mathrm{ev}} \Delta t = E_i^{\mathrm{ev}}, \qquad \forall\ i, t, \tag{3}$$

$$\omega_{i,t} \underline{p}^{\mathrm{ev}} \leq p_{i,t}^{\mathrm{ev}} \leq \omega_{i,t} \overline{p}^{\mathrm{ev}}, \qquad \forall\ i, t. \tag{4}$$

For the battery, the net battery power $p_{i,t}^{\mathrm{b}}$ is defined as the difference between the discharging power $p_{i,t}^{\mathrm{bd}}$ and the charging power $p_{i,t}^{\mathrm{bc}}$, as follows:

$$p_{i,t}^{\mathrm{b}} = p_{i,t}^{\mathrm{bd}} - p_{i,t}^{\mathrm{bc}}, \quad \forall\ i, t. \tag{5}$$

The state of charge of the battery is represented by $e_{i,t}^{\mathrm{b}}$, and the efficiency of charging and discharging are represented by $\eta_{\mathrm{in}}^{\mathrm{b}}$, $\eta_{\mathrm{out}}^{\mathrm{b}}$ respectively. $e_{i,t}^{\mathrm{b}}$ is determined as follows:

$$e_{i,t}^{\mathrm{b}} = e_{i,t-1}^{\mathrm{b}} + p_{i,t}^{\mathrm{bc}} (\eta_{\mathrm{in}}^{\mathrm{b}} - \frac{p_{i,t}^{\mathrm{bd}}}{\eta_{\mathrm{out}}^{\mathrm{b}}}) \Delta(t), \quad \forall\ i, t. \tag{6}$$

$p_{i,t}^{\mathrm{bd}}$, $p_{i,t}^{\mathrm{bc}}$ and $e_{i,t}^{\mathrm{b}}$ are all constrained within upper and lower limits as follows:

$$\underline{p}_i^{\mathrm{bd}} \leq p_{i,t}^{\mathrm{bd}} \leq \overline{p}_i^{\mathrm{bd}}, \quad \forall\ i, t, \tag{7a}$$

$$\underline{p}_i^{\mathrm{bc}} \leq p_{i,t}^{\mathrm{bc}} \leq \overline{p}_i^{\mathrm{bc}}, \quad \forall\ i, t, \tag{7b}$$

$$\underline{e_i^{\mathrm{b}}} \leq e_{i,t}^{\mathrm{b}} \leq \overline{e_i^{\mathrm{b}}}, \quad \forall\ i, t. \tag{7c}$$

Finally, every household has a two-way connection to the microgrid, allowing for withdrawal and injection of real and reactive power. Net power injections into the microgrid are designated as $p_{i,t}$ and $q_{i,t}$, with positive values representing injection and negative values representing withdrawal. $p_{i,t}$ and $q_{i,t}$ are calculated as follows:

$$p_{i,t} = p_{i,t}^{\mathrm{g}} + p_{i,t}^{\mathrm{pv}} + p_{i,t}^{\mathrm{b}} - p_{i,t}^{\mathrm{c}} - p_{i,t}^{\mathrm{ev}}, \qquad \forall\ i, t, \tag{8}$$

$$q_{i,t} = q_{i,t}^{\mathrm{g}} - q_{i,t}^{\mathrm{c}}, \qquad \forall\ i, t. \tag{9}$$

2.2 AC-OPF problem

The complex power flow in line i is denoted as $S_{i,t} = P_{i,t} + \mathtt{i} Q_{i,t}$, where $P_{i,t}$ and $Q_{i,t}$ represent the real and reactive power flow through line i at time t, respectively. The convention is adopted that positive values

represent power flow from i to j, whereas negative values represent power flow from j to i. The squared voltage at node i is represented by $\nu_{i,t} = v_{i,t}^2$ and the squared current magnitude is represented by $\psi_{i,t} = I_{i,t}^2$. These quantities can be related by adopting the branch flow model for modelling the AC power flow in a single phase radial network. The branch flow model is a Second Order Cone (SOC) convex relaxation of the AC-OPF optimization problem [56]. The following equations from the branch flow model are considered:

$$p_{i,t} = P_{i,t} - \sum_{k \in \delta_i} P_{k,t} - r_i \psi_{i,t}, \qquad \forall\ i, t, \tag{10a}$$

$$q_{i,t} = Q_{i,t} - \sum_{k \in \delta_i} Q_{k,t} - x_i \psi_{i,t}, \qquad \forall\ i, t, \tag{10b}$$

$$\nu_{i,t} = \nu_{j,t} + 2(r_i P_{i,t} + x_i Q_{i,t}) - \psi_{i,t}(r_i^2 + x_i^2), \qquad \forall\ i, t, \tag{10c}$$

$$\psi_{i,t} = \frac{P_{i,t}^2 + Q_{i,t}^2}{\nu_{i,t}}, \qquad \forall\ i, t. \tag{10d}$$

The net power balance at node i is given by the departing power quantity minus the arriving power quantities minus the losses. As such, the net real $p_{i,t}$ and reactive $q_{i,t}$ power quantities at node i are given by (10a) and (10b). The squared voltage $\nu_{i,t}$ at node i is given by (10c). Figure 2 illustrates the power flow dynamics in a 4-node example of the proposed radial network. (10d) is a non-convex constraint, and is relaxed to the following inequality [57]:

$$P_{i,t}^2 + Q_{i,t}^2 \leq \psi_{i,t} \nu_{i,t}, \quad \forall\ i, t. \tag{11}$$

Furthermore, the voltage $\nu_{i,t}$ is to be constrained within upper and lower limits, as in (12). Typically these limits are 5% above and below a nominally defined voltage.

$$\underline{\nu} \leq \nu_{i,t} \leq \overline{\nu}, \quad \forall\ i, t. \tag{12}$$

The optimization objective of the present AC-OPF problem is to minimize total costs of grid withdrawal for every household. It is formulated as follows:

$$\begin{aligned} &\text{minimize} && \sum_{t=0}^{T} \sum_{i=0}^{N} C_{i,t}(p_{i,t}^{\mathrm{g}}), \\ &\text{subject to} && (2\mathrm{a}) - (12). \end{aligned} \tag{13}$$

2.3 Trading mechanism

For the trading mechanism, the unified prosumer market proposed by Baroche et al. [46] is adopted. The unified model provides options for implementing either a pool market model or a bilateral trading system. For the purposes of this study the bilateral trading form is used, which includes the designation of a bilateral trading coefficient to every individual trade. This allows participants to declare preferred trading partners, and may also be used to enable product differentiation. Market participants are assumed to behave rationally and non-strategically. Every node in $\mathcal{N}$ is considered to be a separate market agent. In the unified prosumer market model, costs for every separate agent are minimized across their set of connected assets. This includes the costs of trading with the other participants. It is formulated as follows:

$$\text{minimize} \qquad \sum_{t=0}^{T} \sum_{i=0}^{\mathcal{N}} \left[\sum_{a=1}^{\mathcal{A}} f_{i,t}^{a}(p_{i,t}^{a}) + \sum_{j=0}^{\mathcal{M}} \gamma_{ij,t} |d_{ij,t}| \right], \tag{14a}$$

$$\text{subject to} \qquad \boldsymbol{D}_t = -\boldsymbol{D}_t^{\intercal} \qquad [\boldsymbol{\Xi}_t] \qquad \forall\ t \tag{14b}$$

$$, \qquad \sum_{a=1}^{\mathcal{A}} p_{i,t}^{a} = \sum_{j=0}^{\mathcal{M}} d_{ij,t} \qquad \forall\ i, t, \tag{14c}$$

$$p_{i,t}^{a} \in \mathcal{P}_{i,t}^{a} \qquad \forall\ a, i. \tag{14d}$$

In this formulation, $\mathcal{A}$ indexed by a represents the set of assets of agent i, and $\mathcal{M}$ indexed by j represents the set of trading partners of agent i. $f^a_{i,t}$ represents the cost function of asset a as a function of the power set point $p^a_{i,t}$. $\gamma_{ij,t}$ represents the bilateral trading coefficient imposed by agent i on the trade between agents i and j, and $d_{ij,t}$ is the quantity of electricity traded between agents i and j in timestep t. The matrix $\boldsymbol{D}$ contains the quantities of all trades, and the associated dual variable matrix $\boldsymbol{\Xi}$ contains the prices of all trades. Set $\mathcal{P}^a_{i,t}$ contains the feasible set of power set points of i at t. Constraint (14b) enforces reciprocity of trade quantities, and reciprocity of trading prices $\boldsymbol{\Xi}$ is also implicitly enforced by this constraint as it is the dual variable. Constraint (14c) ensures that the sum of all power generated by agent i equals the sum of the quantities of all trades conducted. It can be recognized that low values of the bilateral trading coefficient $\gamma_{ij,t}$ indicate preferred trading partners whereas high values represent undesirable trading partners. In the current study the only source of costs for every agent besides trading is the external grid connection, of which the costs function is (1). As such, in a trade-only scenario where grid constraints are not considered, the optimization problem can be rewritten as:

$$\begin{aligned}
&\text{minimize} && \sum_{t=0}^{T}\sum_{i=0}^{\mathcal{N}}\left[C_{i,t}(p^{\mathrm{g}}_{i,t}) + \sum_{j=0}^{\mathcal{M}}\gamma_{ij,t}|d_{ij,t}|\right], && && (15a)\\
&\text{subject to} && \boldsymbol{D}_t = -\boldsymbol{D}_t^{\intercal} && [\boldsymbol{\Xi}_t] && \forall\ t, && (15b)\\
& && p_{i,t} = \sum_{j=0}^{\mathcal{M}} d_{ij,t} && && \forall\ i,t, && (15c)\\
& && (2\mathrm{a}), (3)-(8). && && &&
\end{aligned}$$

2.4 Decentralized formulation

2.4.1 General consensus ADMM

In order to solve the optimization problem in a distributed manner, the general consensus optimization form of the ADMM algorithm is used. The global optimization problem is split in a number of subproblems $f_1(x_1) + f_2(x_2) + \ldots + f_n(x_n)$ where each agent on the network solves their subproblem locally and in parallel. Accordingly, the variables are split into sets of local variables $x_1, x_2, \ldots, x_n$ where each set of local variables is needed to solve the corresponding local subproblem. Every set of local variables consists of a number of components $(x_i)_c$, each of which corresponds to a component $(z_g)_c$ of the set of global variables z_g. The set of global variables contains all variables that are used in the global optimization problem and is used ensure consensus between all agents as they come to a consensus on the value of every global variable component. For some global variable components, there is only one corresponding local variable component in one subproblem: in these cases, the consensus procedure is not needed. For other global variable components, there are two or more corresponding local variable components across an equal number of subproblems, and consensus must be ensured. Accordingly, every set of local variables x_l is split into a set of local private variables $(x_l)_i$, which contains variables that are specific to that agent and subproblem only, and a set of local coupling variables $(x_u)_i$, which contains variables that are shared between two or more agents and are thus used to couple the different subproblems together. Consensus across the entire network is achieved when every local variable component $(x_i)_c$ is equal to the corresponding global variable component $(z_g)_c$. Using notation from [53], this consensus condition can be formulated as:

$$(x_i)_c = z_{\mathcal{G}(i,c)}, \quad \forall\ i, c. \tag{16}$$

We define the variable $(\tilde{z}_i)_c$ which is equal $z_{\mathcal{G}(i,c)}$, and define the consensus constraint as $x_i - \tilde{z}_i = 0$. As such, the general form consensus problem can be written as follows:

$$\begin{aligned}
&\text{minimize} && \sum_{i=0}^{\mathcal{N}} f_i(x_i), && \forall\ i,t, && (17\mathrm{a})\\
&\text{subject to} && x_i - \tilde{z}_i = 0, && \forall\ i,t. && (17\mathrm{b})
\end{aligned}$$

Then, the augmented Lagrangian of this problem is formulated as:

$$L_\rho(x,z,y) = \sum_{i=0}^{\mathcal{N}} (f_i(x_i) + y_i^\intercal (x_i - \tilde{z}_i) + (\rho/2)\left\|x_i - \tilde{z}_i\right\|_2^2), \tag{18}$$

where y represents the dual variable, and ρ represents the penalty parameter (i.e. the step size) which is predefined. In (18), it can be recognized that minimizing the second and third terms enforces constraint (17b). In the general consensus ADMM algorithm, (18) is solved through a series of iterative steps, in each of which the x, y and z variables are determined separately. When calculating each of these variables, the most recently calculated values of the other two are used to do so. As such, in every iteration $k+1$, following derivation in [53], the three steps are then formulated as:

$$x_i^{k+1} = \underset{x_i}{\operatorname{argmin}} (f_i(x_i) + y_i^{k\intercal} (x_i - \tilde{z}_i^k) + (\rho/2)\left\|x_i - \tilde{z}_i^k\right\|_2^2), \tag{19a}$$

$$z_g^{k+1} = (1/k_g) \sum_{\mathcal{G}(i,c)=g} (x_i^{k+1})_c, \tag{19b}$$

$$y_i^{k+1} = y_i^k + \rho(x_i^{k+1} - \tilde{z}_i^{k+1}). \tag{19c}$$

In (19b), k_g represents the number of local variable components that correspond to z_g. It can be recognized that (19b) is essentially an averaging of all local variable components to retrieve the corresponding global variable component. In the dual variable update (19c), it can be recognized that the larger the difference between the local and global variables x_i and $\tilde{z}_i$, the larger the magnitude of the y update will be, and thus the more strongly the constraint (17b) will be enforced in (19a).

The ADMM algorithm will iterate through the steps until the convergence conditions are met. These conditions are evaluated through the primal and dual residual values r^k and s^k, which are defined as follows:

$$r^k = x_i^k - \tilde{z}_i^k, \tag{20a}$$

$$s^k = z_g^k - z_g^{k-1}. \tag{20b}$$

The convergence conditions are then defined as:

$$\left\|r^k\right\|_2 \leq \epsilon_p, \tag{21a}$$

$$\left\|s^k\right\|_2 \leq \epsilon_d. \tag{21b}$$

In (21a) and (21b), ϵ_p and ϵ_d are the allowed tolerances for the primal and dual residuals respectively, which are typically assigned a low value in the range of $10^{-2} - 10^{-3}$. Besides meeting the convergence conditions, the execution of and ADMM algorithm is also typically assigned a maximum number of iterations after which execution of the algorithm will end.

2.4.2 ADMM and AC-OPF

The AC-OPF of (13) is reformulated using the general consensus form ADMM. The global optimization problem is decomposed into a set of subproblems where every node $i \in \mathcal{N}$ solves its own local subproblem using its own set of local variables x_i. In this set of local variables, the subset of local private variables $(x_l)_i := [p_i, p_i^{\mathrm{g}}, q_i, q_i^{\mathrm{g}}, \psi_i, p_i^{\mathrm{b}}, p_i^{\mathrm{bc}}, p_i^{dc}, e_i^{\mathrm{b}}, p_i^{\mathrm{ev}}]$ generally contains the variables pertaining to local energy infrastructure and the set of coupling variables $(x_u)_i := [P_i, Q_i, v_i, P_{\delta(i)}, Q_{\delta(i)}, v_{\pi(i)}]$ generally contains the variables pertaining to its set of branch flow equations. The set of global variables is denoted as $z_g := [P, Q, v]$. Since for every node the set of coupling variables only contains variables that are related to itself or the neighbouring edges and nodes, the full network topology will not have to be known by any node. Every node must only know who its neighbouring nodes (i.e. parent and children) are. Figure 3 shows how the locally calculated coupling variables correspond to the global variables in the present OPF problem. The local subproblem for a node i looks as follows:

$$\begin{aligned} &\text{minimize} && C_{i,t}(p_{i,t}^{\mathrm{g}}), \\ &\text{subject to} && (2\mathrm{a}) - (12). \end{aligned} \tag{22}$$

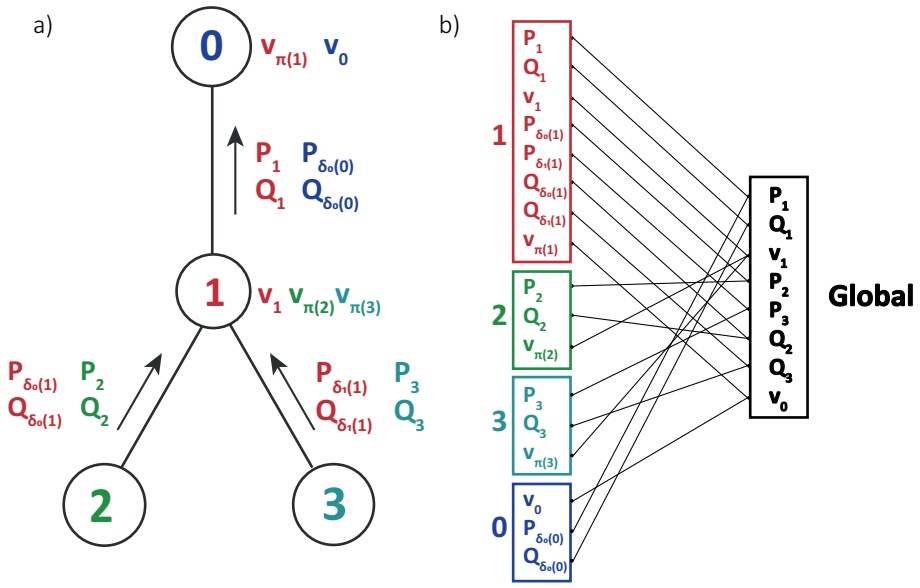

Figure 3: An illustration of the coupling between local and global variables in the ADMM-based general form consensus method for the OPF problem in a 4-nodes network.

The steps of the ADMM algorithm are executed according to (19a) - (19c). In iteration $k+1$ every node i first receives z_g^k and solves the following local optimization problem:

$$\text{minimize} \quad C_{i,t}(p_{i,t}^{\text{g}}) + y_i^{k\intercal}(x_i - \tilde{z}_i^k) + (\rho/2)\left\|x_i - \tilde{z}_i^k\right\|_2^2. \tag{23}$$

The nodes then exchange the coupling variables with the aggregator and z is updated as:

$$z_g^{k+1} := (1/k_g) \sum_{\mathcal{G}(i,c)=g} (x_i^{k+1})_c. \tag{24}$$

The nodes then receive $\tilde{z}_i^{k+1}$ and update the penalty locally as:

$$y_i^{k+1} = y_i^k + \rho(x_i^{k+1} - \tilde{z}_i^{k+1}). \tag{25}$$

Finally, primal and dual residual values r_g^{k+1} and s_g^{k+1} are defined:

$$r_{\text{grid}}^{k+1} = \sum_{i=0}^{\mathcal{N}} x_i^k - \tilde{z}_i^k, \tag{26a}$$

$$s_{\text{grid}}^{k+1} = \sum_{i=0}^{\mathcal{N}} z_g^k - z_g^{k-1}. \tag{26b}$$

2.4.3 ADMM and trading mechanism

As for the OPF problem, the optimization problem (14a) is decomposed into subproblems where every agent solves their corresponding subproblem. Every agent will determine their own local trading schedule $\boldsymbol{D}$, which is treated as a coupling variable that corresponds to the global variable $\boldsymbol{C}$. Following [46], $\boldsymbol{C} = (\boldsymbol{D} - \boldsymbol{D}^\intercal)/2$ is defined as the average of the trading quantity proposed by agent i to agent j and the trading quantity proposed by agent j to agent i. Since the global variable $\boldsymbol{C}$ is skew-symmetric, it can be rewritten as

$(\boldsymbol{C} - \boldsymbol{C}^{\intercal})/2 = \boldsymbol{D}$. By using this consensus constraint, the fully decentralized augmented Lagrangian for bilateral trading can be formulated as follows:

$$\begin{aligned}
\big(p_i^{\mathrm{g}}, D_i\big)^{k+1} = \quad & \underset{p_i^{\mathrm{g}}, T_i}{\operatorname{argmin}} && \sum_{t=0}^{\mathcal{T}} \Bigg[C_{i,t}^{\mathrm{g}}(p_{i,t}^{\mathrm{g}}) + \sum_{j=0}^{\mathcal{M}} \Bigg[\gamma_{ij,t} |d_{ij,t}^{k+1}| + \\
& && (\phi/2) \Big(\frac{d_{ij,t}^{k} - d_{ji,t}^{k}}{2} - d_{ij,t}^{k+1} + \xi_{ij,t}^{k}/\phi \Big)^2 \Bigg] \Bigg], && \text{(27a)} \\
& \text{subject to} && p_{i,t} = \sum_{j=0}^{\mathcal{M}} d_{ij,t}, && \text{(27b)} \\
& && \text{(2a)}, (3) - (8). &&
\end{aligned}$$

In this formulation the penalty parameter is represented by ϕ. Dual variable ξ, representing the price of trading, being updated in the next step:

$$\xi_{ij,t}^{k+1} = \xi_{ij,t}^{k} - \rho(d_{ij,t}^{k+1} + d_{ji,t}^{k+1})/2. \tag{28}$$

Finally, residuals are calculated as follows:

$$r_{\text{trade}}^{k+1} = \sum_{i=0}^{\mathcal{N}} \sum_{t=0}^{T} \sum_{j=0}^{\mathcal{M}} \big(d_{ij,t}^{k+1} + d_{ji,t}^{k+1}\big)^2, \tag{29a}$$

$$s_{\text{trade}}^{k+1} = \sum_{i=0}^{\mathcal{N}} \sum_{t=0}^{T} \sum_{j=0}^{\mathcal{M}} \big(d_{ij,t}^{k+1} - d_{ij,t}^{k}\big)^2. \tag{29b}$$

2.4.4 Combined formulation

As stated, the main contribution of this study is the combination of an OPF problem with a trading mechanism in a single distributed optimization problem. This leads to a fully decentralized algorithm that achieves maximum total social welfare by minimizing both grid withdrawal costs and trading costs for every agent $i \in \mathcal{N}$ separately and in parallel while respecting global grid constraints and balancing the market. The fully decentralized algorithm consists of several iterative steps. First, the local optimization problem is solved by agent i:

$$\begin{aligned}
\big(x_i, \boldsymbol{D}_i\big)^{k+1} = \quad & \underset{x_i, T_i}{\operatorname{argmin}} && \sum_{t=0}^{T} \Bigg[C_{i,t}^{\mathrm{g}}(p_{i,t}^{\mathrm{g}}) + y_{i,t}^{k\intercal}(x_{i,t} - \tilde{z}_{i,t}^{k}) + (\rho/2) \left\| x_{i,t} - \tilde{z}_{i,t}^{k} \right\|_2^2 \\
& && + \sum_{j=0}^{\mathcal{M}} \Bigg[\gamma_{ij,t} |d_{ij,t}^{k+1}| + (\phi/2) \Big(\frac{d_{ij,t}^{k} - d_{ji,t}^{k}}{2} - d_{ij,t} + \xi_{ij,t}^{k}/\phi \Big)^2 \Bigg] \Bigg], && \text{(30)} \\
& \text{subject to} && \text{(2a)} - (12), \text{(27b)}. &&
\end{aligned}$$

It can be recognized that two separate penalty parameters are used, ρ for the grid constraints and ϕ for the trading mechanism. In this first step, agent i calculates both the set of local variables x_i and the optimal trading schedule $\boldsymbol{D}$ for every timestep. In the next step, the global variables z_g are calculated:

$$z_g^{k+1} := (1/k_g) \sum_{\mathcal{G}(i,c)=g} (x_i^{k+1})_c. \tag{31}$$

In the third step, dual variables y and ξ are updated by every agent:

$$\xi_{ij,t}^{k+1} = \xi_{ij,t}^{k} - \phi(d_{ij,t}^{k+1} + d_{ji,t}^{k+1})/2, \qquad \forall\ j, t, \tag{32a}$$

$$y_i^{k+1} = y_i^{k} + \rho(x_i^{k+1} - \tilde{z}_i^{k+1}). \tag{32b}$$

After every iteration, separate sets of residuals for grid constraints and trading are calculated as follows:

$$r_{\text{grid}}^{k+1} = \sum_{i=0}^{\mathcal{N}} x_i^k - \tilde{z}_i^k, \tag{33a}$$

$$s_{\text{grid}}^{k+1} = \sum_{i=0}^{\mathcal{N}} \tilde{z}_i^k - \tilde{z}_i^{k-1}, \tag{33b}$$

$$r_{\text{trade}}^{k+1} = \sum_{i=0}^{\mathcal{N}} \sum_{t=0}^{T} \sum_{j=0}^{\mathcal{M}} \left(d_{ij,t}^{k+1} + d_{ji,t}^{k+1}\right)^2, \tag{33c}$$

$$s_{\text{trade}}^{k+1} = \sum_{i=0}^{\mathcal{N}} \sum_{t=0}^{T} \sum_{j=0}^{\mathcal{M}} \left(d_{ij,t}^{k+1} - d_{ij,t}^{k}\right)^2. \tag{33d}$$

2.5 Blockchain implementation

By using blockchain and smart contracts technology the proposed distributed algorithm can be executed in a secure, verifiable manner that ensures independence and anonimity of the network participants. In such a setup, the role of the smart contract is essential. A smart contract is a piece of computer code that is deployed on the blockchain and can execute certain functions when called upon by other nodes [26] [24]. Smart contract technology allows decentralized optimization on a blockchain network, enabling execution of the distributed algorithm without dependence on a central agent (e.g., a third party aggregator). The smart contract takes over the function of this central aggregator, thus effectively functioning as a virtual aggregator. In this role, the smart contract acts as the primary agent for nodes to interact with during execution. It should be emphasized that the smart contract is not a computer programme that is executed as a whole, nor does it loop through the ADMM algorithm steps. Rather it is a collection of functions that are executed when called upon by other nodes. As a virtual aggregator, the smart contract performs several types of functions:

1. Executing parts of the ADMM algorithm
2. Exchanging information with other nodes
3. Giving permission to other nodes to proceed with the next operation.

Various steps in the ADMM algorithm are distinguished where these functions are executed. The smart contract is written in the Solidity language, which is the most commonly used for smart contracts, and the other files that are run locally are written in Python. The Python package Web3.py [58] is used to communicate between the local files and the contract, and the local optimization problem are solved using the Cvxpy package [59]. The blockchain network is set up by running a local Ethereum node with Ganache-cli [60]. It should be noted that the proposed blockchain setup is not assessed for efficiency of communication, security and execution speed. Furthermore, The inherent built-in delay in the blockchain verification process may make the use of blockchain for real-time optimization implausible or impractical. Therefore, the model proposed in this study is intended to provide a day-ahead forecast optimization of energy flows.

Upon setting up the blockchain network every node i is assigned a personal account with address λ_i. This account is used to interact with the network and send/retrieve data to/from the smart contract. The smart contract $\boldsymbol{\sigma}$ is deployed to the network using a configuration file. This action only has to be performed once by a single node: the contract remains on the network indefinitely after deployment. This is done using a set of constructor variables $\theta := [n, \rho, \phi, \epsilon_p^{\text{g}}, \epsilon_d^{\text{g}}, \epsilon_p^t, \epsilon_d^t, \mu]$ that configure the ADMM algorithm. The variable μ represents the maximum number of iterations, n represents the total number of nodes on the network. It can be noted that it is not required to pass any information on the network topology. As the contract is deployed, a new address $\lambda_{\boldsymbol{\sigma}}$ and the bytecode of the contract's contents $ABI_{\boldsymbol{\sigma}}$ are generated. $\lambda_{\boldsymbol{\sigma}}$ and $ABI\boldsymbol{\sigma}$ must be known by all other nodes to allow them to interact with the contract.

In the execution of the ADMM algorithm on the blockchain network for OPF there are several steps that can be distinguished where there is communication between the smart contract $\boldsymbol{\sigma}$ and the nodes $i \in \mathcal{N}$. The various steps are visualised in Figure 4.

1. In step 1, i connects to $\boldsymbol{\sigma}$ by using the adress $\lambda_{\boldsymbol{\sigma}}$ and bytecode ABI_σ. This action only has to be performed once.

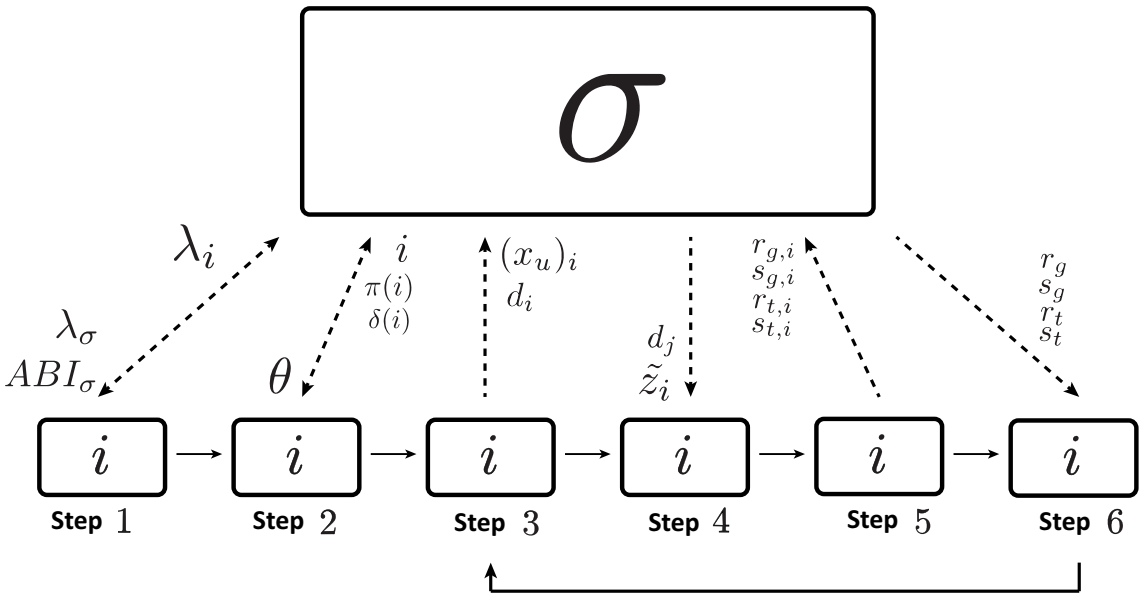

Figure 4: A flowchart showing the interaction between the smart contract σ and node i in the steps of the ADMM algorithm.

2. In step 2 a new round of optimization starts for the next day, and all nodes will declare their participation to the smart contract by passing its number i and the numbers of their parent node $\pi(i)$ and children nodes $\delta(i)$. Also, the nodes will retrieve θ from the contract to configure the local optimization problem. As the nodes declare participation, $\boldsymbol{\sigma}$ keeps track using a counter. In the meantime, the nodes will periodically call a checking function to check if all n nodes have connected. When all n nodes have declared participation, the nodes will proceed to solve their local optimization problem.

3. When local optimization (30) is complete, the nodes send their sets of coupling variables $(x_u)_i$ and their set of trade bids d_i to the smart contract which will keep track using a counter, and wait for further instructions by calling a checking function. When all nodes submitted their coupling variables, one node is configured to call the z-update step function, which will make the contract execute (31) of ADMM. Note that the set of trade bids contains the optimally calculated trading quantities for all trading partners and all timesteps. For the trading portion, the only role of the smart contract is to gather all trade bids and distribute them to the respective trading partners. While the contract executes the z-update, all nodes periodically call checking functions to check if the smart contract has completed its task.

4. When the z-update step is complete, the nodes will retrieve the recalculated global variables as well as the trade bids of their trading partners d_j. The nodes will form their full trading quantity matrix $d_{ij,t}$ from d_i and d_j and calculate their local penalty values (32a) (32b). The nodes will also calculate the partial residual values as in (33a) - (33d) for their local problem.

5. The nodes send the partial residuals to the contract, which initiates a counter and sums all partial residuals upon completion to receive the global residuals. The nodes periodically call checking functions to check for completion.

6. The nodes retrieve the global residual values and evaluate the converge conditions. If the conditions are not satisfied, go back to step 3) and repeat.

It can be recognized that very little sensitive information is shared by the nodes with the contract. All information regarding the local energy infrastructure (i.e. local private variables $(x_l)_i$) remains private: only data on power flows in adjacent lines is shared, as well as residual values and trade bids. This information is stored on the smart contract, and not accessible by any other nodes on the network. Furthermore, it can be recognized that full network topology is not explicitly stated anywhere. Every node must only know which nodes its parent and children are. As all nodes share this information with the contract, the full network topology will be implicitly known by it.

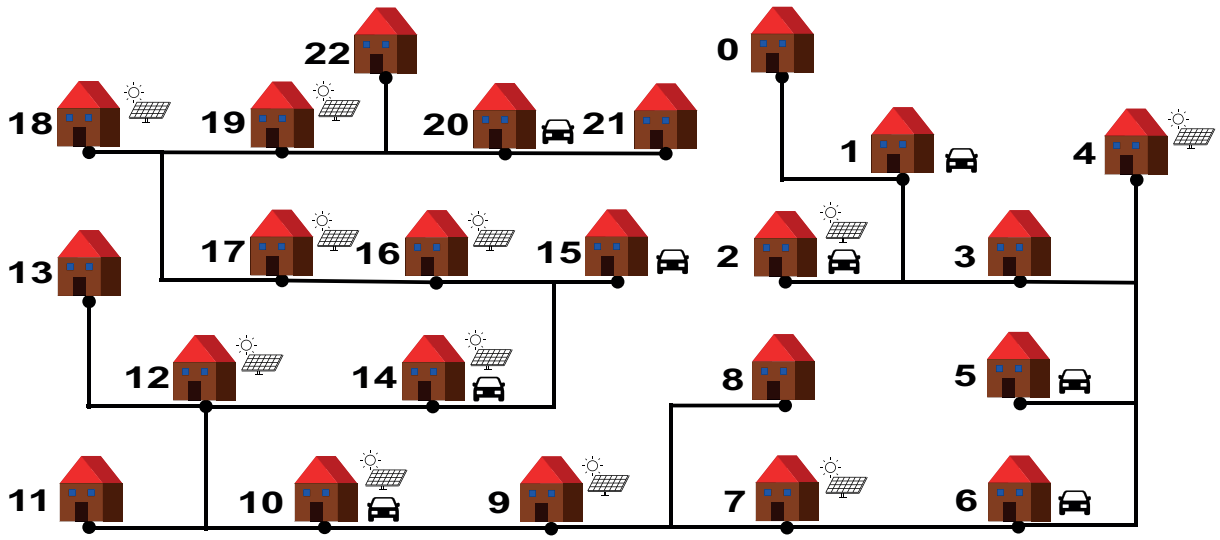

Figure 5: Topology of the considered microgrid. Owners of EV and PV are indicated.

2.6 Numerical Analysis

For the fixed real power load and solar generation data, real data from the East Harbour Prosumers Community [61] in Amsterdam is used in order to give a realistic assessment of the viability of the proposed model in a microgrid setup. The fixed reactive power load is assumed to be proportional to $-1/10$th of the real power load. For the topology and parameters of the radial microgrid, data from the test network of [62] is used. Figure 5 shows the topology of the radial grid. For grid electricity withdrawals, a time-of-use price signal κ_t is used from the day-ahead market clearing prices of the European Power Exchange (EPEX) Netherlands [63]. The lower limit of real power generation $\underline{p}^{\mathrm{g}}$ is set at 0 and the upper limit $\overline{p}^{\mathrm{g}}$ is set at 6.5kW [64]. It is assumed that each household with EV drives 36 km each day, which is the average daily distance travelled in the Netherlands [65], with a driving efficiency of 5 km per kWh. This results in an average EV daily charging demand (E_{ev}) of 7.06 kWh. The maximum hourly charging rate is assumed to be 1.5 kWh. The charging hours ω_i are pre-defined, with some households preferring to charge during the day and others during the night. Every household that has access to solar PV also owns a battery storage system, with the maximum charge/discharge rates $\overline{p}_i^{\mathrm{bd}}$, $\overline{p}_i^{\mathrm{bc}}$ being equal to half of the maximum energy generation of the PV installation. The maximum (dis)charge rate for every household is shown in Table 1. The minimum stae of charge of the battery $\underline{e}_i^{\mathrm{b}}$ is equal to 1/5th of 4 hours of maximum charging, as $0.2(4\overline{p}_i^{\mathrm{bc}})$, and the maximum state of charge of the battery $\overline{e}_i^{\mathrm{b}}$ is equal to 4/5th of 4 hours of maximum charging, as $0.8(4\overline{p}_i^{\mathrm{bc}})$. Table 1 shows the metadata for the setup of all households that are considered, and Figure 5 shows the locations of PV and EV owners in the grid.

The bilateral trading coefficients are pre-determined for every household based on their fixed real power consumption and solar PV generation data. Since the model is intended to provide a day-ahead forecasting optimization, it is assumed that a forecast of their own consumption and generation is available to the households. It is assumed that the willingness to trade of a household i in any timestep t is proportional to the magnitude of their expected deficit/surplus $p_{i,t}^{c} - p_{i,t}^{\mathrm{pv}}$. It is assumed that households with an expected surplus budget are more likely to trade with households that have an expected deficit and visa versa. Two households that both have a deficit or both have a surplus are assumed to be very unlikely trading partners. In order to reflect these assumptions in the bilateral trading coefficients, several steps are taken.

First, the expected net budget matrix $\boldsymbol{P}^{\mathrm{net}}$ is determined. Along the x_1 axis it contains all households and is indexed by i, and along the x_2 axis it contains all timesteps and is indexed by t. $\boldsymbol{P}^{\mathrm{net}}$ is defined as:

$$\boldsymbol{P}^{\mathrm{net}} = \boldsymbol{P}^{\mathrm{pv}} - \boldsymbol{P}^{\mathrm{c}} \tag{34}$$

From matrix $\boldsymbol{P}^{\mathrm{net}}$, two new matrices $\boldsymbol{P}^{\mathrm{buy}}$ and $\boldsymbol{P}^{\mathrm{sell}}$ are defined. These matrices contain the amount of

power that each household wants to sell or buy in every timestep. They are determined as follows:

$$p_{it}^{\text{buy}} = \begin{cases} 0 & \text{if } p_{it}^{\text{net}} \geq 0 \\ p_{it}^{\text{net}} & \text{if } p_{it}^{\text{net}} < 0 \end{cases} \tag{35a}$$

$$p_{it}^{\text{sell}} = \begin{cases} p_{it}^{\text{net}} & \text{if } p_{it}^{\text{net}} > 0 \\ 0 & \text{if } p_{it}^{\text{net}} \leq 0 \end{cases} \tag{35b}$$

From these matrices, two column vectors $\overline{P}_{\text{max}}^{\text{buy}}$ and $\overline{P}_{\text{max}}^{\text{sell}}$ are defined. Each element of these vectors represents the maximum value in the corresponding row of the matrices $\boldsymbol{P}^{\text{buy}}$ and $\boldsymbol{P}^{\text{sell}}$. This means that these vectors contain the maximum deficit and surplus budget of every household across all timesteps. $\boldsymbol{P}^{\text{buy}}$ and $\boldsymbol{P}^{\text{sell}}$ are then normalized as:

$$\boldsymbol{\Gamma}^{\text{b,rel}} = \frac{\chi}{2} \frac{\boldsymbol{P}^{\text{buy}}}{\overline{P}_{\text{max}}^{\text{buy}}} \tag{36a}$$

$$\boldsymbol{\Gamma}^{\text{s,rel}} = \frac{\chi}{2} \frac{\boldsymbol{P}^{\text{sell}}}{\overline{P}_{\text{max}}^{\text{sell}}} \tag{36b}$$

Matrices $\boldsymbol{\Gamma}^{\text{b,rel}}$ and $\boldsymbol{\Gamma}^{\text{s,rel}}$ represent the relative willingness of households to buy or sell electricity. Parameter χ represents the maximum, baseline value for bilateral trading coefficients. From matrices $\boldsymbol{\Gamma}^{\text{b,rel}}$ and $\boldsymbol{\Gamma}^{\text{s,rel}}$, the final 3D matrix of bilateral trading coefficients $\boldsymbol{\Gamma}$ is defined as follows:

$$\gamma_{ij,t} = \begin{cases} \chi & \text{if } \gamma_{it}^{\text{s,rel}} > 0 \text{ and } \gamma_{jt}^{\text{s,rel}} > 0 \\ \chi & \text{if } \gamma_{it}^{\text{b,rel}} > 0 \text{ and } \gamma_{jt}^{\text{b,rel}} > 0 \\ \chi - (\gamma_{it}^{\text{b,rel}} + \gamma_{jt}^{\text{b,rel}} + \gamma_{it}^{\text{s,rel}} + \gamma_{jt}^{\text{s,rel}}) & \text{otherwise} \end{cases} \tag{37}$$

At the maximum value of $\gamma_{ij,t} = \chi$, nodes i and j are considered very unlikely trading partners. In the present study, χ is set at 10, meaning that all bilateral trading coefficients have a value of anywhere between 0 and 10. In order to assess performance of the integrated model, several scenarios are considered and compared. First, the penalty variable for the trading portion of the model ϕ will be varied to assess its impact on the convergence of the ADMM algorithm and the costs of trading. These scenarios are run for 1 day (21 June 2018), i.e. 24 timesteps of 1 hour. Based on the results gained from these initial runs, the ϕ value that yields the best convergence is used for further testing.

In order to evaluate the impact of including the bilateral trading mechanism and grid constraints on convergence, social welfare and scheduling of power flows and trading scheme, several scenarios are compared where these different parts of the model are included and excluded. A baseline model will also be analysed, where there is no microgrid and households only interact with the external grid. In this baseline model prosumers are able to feed their excess electricity budget into the grid for 5 ct/kWh. These scenarios are run for one week in summer (21-28 June 2018) and one week in winter (21-28 December 2018) to evaluate performance in both seasons.

The scenarios that include both trade and grid portions execute the optimization problem as in (30) - (33d). Scenarios with grid only execute the problem as in (22) - (25) and scenarios with trade only execute the problem as in (27a) - (28). All scenarios that are compared are shown in Table 2.

Code	#	**PV**	**EV**	$\overline{p^{\mathrm{b}}}(kW)$
1011W	0	No	No	0
1954W	1	No	Yes	0
1964J	2	Yes	Yes	1.39
2053G	3	No	No	0
2442E	4	Yes	No	0.79
3070L	5	No	Yes	0
3307S	6	No	Yes	0
3517V	7	Yes	No	0.53
3660D	8	No	No	0
3726A	9	Yes	No	1.41
3932W	10	Yes	Yes	0.51
4226R	11	No	No	0
4451M	12	Yes	No	2.44
5427W	13	No	No	0
5815T	14	Yes	Yes	1.58
7426U	15	No	Yes	0
7679U	16	Yes	No	1.47
7710F	17	Yes	No	1.47
8319Q	18	Yes	No	1.25
9248C	19	Yes	No	0.46
9370J	20	No	Yes	0
9506H	21	No	No	0
9991J	22	No	No	0

Table 1: Household metadata

Code	#	**Scenario**
TG0001	1	$\phi = 0.001$
TG001	2	$\phi = 0.01$
TG01	3	$\phi = 0.1$
TG1	4	$\phi = 1$
TG10	5	$\phi = 10$
TG100	6	$\phi = 100$
TG1000	7	$\phi = 1000$
TGS	8	Trade + Grid, summer
TGW	9	Trade + Grid, winter
GS	10	Grid only, summer
GW	11	Grid only, winter
TS	12	Trade only, summer
TW	13	Trade only, winter
BS	14	Baseline, summer
BW	15	Baseline, winter

Table 2: Scenarios of the model

3 Results

The objective of this study is to assess the performance of the integrated model in several categories: convergence of the ADMM algorithm, social welfare and scheduling of power flows and trading scheme. In order to perform this assessment several performance parameters are used in every category.

For assessment of convergence of the ADMM algorithm, the different scenarios are all run for $\mu = 300$ iterations. After 300 iterations the residual values, both for grid and trade portions, are evaluated and compared between the scenarios. The convergence of residuals for all scenarios can be seen in Figure 6. The residual values shown represent the combined total residuals for all households. The convergence for scenarios 1-7 are for model runs of 1 day. Based on these results, a ϕ value of 1000 is chosen for running scenarios 8-15, which are run for 1 week. All subsequent results are based on these 1 week runs of scenarios 8-15.

Scheduling of power flows and trading of all scenarios is visualised in Figures 7, 8, 9, 10, 13 and 14. Figure 7 shows the magnitude of the total sum of a number of energy flows, including total consumption, total grid withdrawals, total PV generation and total battery and EV consumption for the 1st day of the week. Full-week versions of these graphs can be found in appendix A. The scheduling of the energy flows is compared for all scenarios. Figure 8 shows the exchange of power in the grid, split up in the total volume of electricity withdrawn externally and the total volume of electricity traded internally. Results for these figures are only shown for day 1 of the week. Numerical values for the total sum across the entire week for power withdrawn, in total and at peak hours, are found in Table 3. Figures 9 and 10 show the total amount of power traded between the nodes over the whole week. A comparison is made with the bilateral trading coefficients, which are averaged across all timesteps of the entire week. Finally, Figures 13 and 14 show the power injections and voltage levels in the microgrid for day 1.

In the social welfare category the performance parameters represent financial costs for the households. Figure 11 shows the total social welfare for scenarios 8-15, with costs split up into money spent on withdrawals from the external grid and money spent on internal trades. Figure 12 shows the price of electricity across the entire week, both of internal trading and external grid withdrawals. Table 3 shows numerical values of total social welfare across the entire week. In this table, a comparison is made between total prosumer costs and total consumer costs. These costs are summed for all prosumers and consumers respectively.

	Summer				Winter			
Scenario	BS	GS	TS	TGS	BW	GW	TW	TGW
Prosumer grid costs (Eur)	112.88	8.97	54.49	61.25	234.92	98.01	225.20	228.70
Consumer grid costs (Eur)	95.24	114.17	54.14	66.96	227.81	368.18	217.26	232.81
Prosumer trade costs (Eur)	–	–	-41.21	-28.65	–	–	-1.45	-1.17
Consumer trade costs (Eur)	–	–	41.21	28.65	–	–	1.45	1.17
Total prosumer costs (Eur)	112.88	8.97	13.28	32.60	234.93	98.01	223.77	227.53
Total consumer costs (Eur)	95.24	114.17	94.85	95.46	227.81	363.18	218.71	233.64
Total grid costs (Eur)	208.22	123.28	108.76	128.35	462.84	466.30	442.58	461.63
Total trade costs (Eur)	–	–	41.21	28.65	–	–	1.45	1.17
Total costs (Eur)	208.22	123.27	156.10	161.06	462.84	466.30	444.12	465.10
Total withdrawal (kWh)	1231	915	741	862	2578	2569	2460	2572
Peak withdrawal (kWh)	333	139	186	211	796	854	738	770
Ratio of peak/total withdrawal	0.27	0.15	0.25	0.24	0.30	0.33	0.30	0.29

Table 3: Numerical results for social welfare and external grid withdrawals. All costs are summed over the entire week and over all households. Prosumer and consumer costs are summed over all prosumer and consumer households respectively. External grid withdrawals are also summed over the entire week and over all households. Peak hours are defined as 6-9am in the morning and 5-8pm in the evening, and peak withdrawals are summed over all peak hours for all days and all households.

Table 4 shows the relative increase or decrease between scenarios in costs and withdrawals of all values shown in 3. Results from the baseline scenarios BS and BW are set as 100%. For the trade costs, results from TS and TW are set as 100%.

	Summer				Winter			
Scenario	BS	GS	TS	TGS	BW	GW	TW	TGW
Relative prosumer grid costs	100%	8.0%	48.3%	54.3%	100%	41.7%	95.9%	97.4%
Relative consumer grid costs	100%	119.7%	56.8%	70.3%	100%	159.2%	95.7%	102.19%
Relative prosumer trade costs	–	–	100%	69.5%	–	–	100%	80.7%
Relative consumer trade costs	–	–	100%	69.5%	–	–	100%	80.7%
Relative total prosumer costs	100%	7.9%	11.8%	28.9%	100%	41.7%	95.24%	96.9%
Relative total consumer costs	100%	119.8%	99.5%	100%	100%	159.2%	96.0%	102.8%
Relative total grid costs	100%	59.2%	52.2%	77.4%	100%	100.7%	95.6%	99.7%
Relative total trade costs	–	–	100%	69.5%	–	–	100%	80.7%
Relative total costs	100%	59.2%	75.0%	77.3%	100%	100.7%	95.6%	100.5%
Relative total withdrawal	100%	74.3%	60.1%	70%	100%	99.7%	95.4%	99.8%
Relative peak withdrawal	100%	41.7%	55.9%	63.4%	100%	107.3%	92.7%	96.7%
Relative ratio of peak/total	100%	55.6%	92.6%	88.9%	100%	110%	100%	96.7%

Table 4: Relative costs and withdrawals as compared to the baseline scenarios, the values of which are set at 100%. For the trade costs, the values of the trade-only scenarios is set at 100%.

Based on the results shown in the figures and tables, a comparison can be made between the different scenarios for every performance category. Building on this, the respective benefits and downsides of the scenarios can be discussed, as well as their applicability in real-life communities. This analysis is made in section 4.

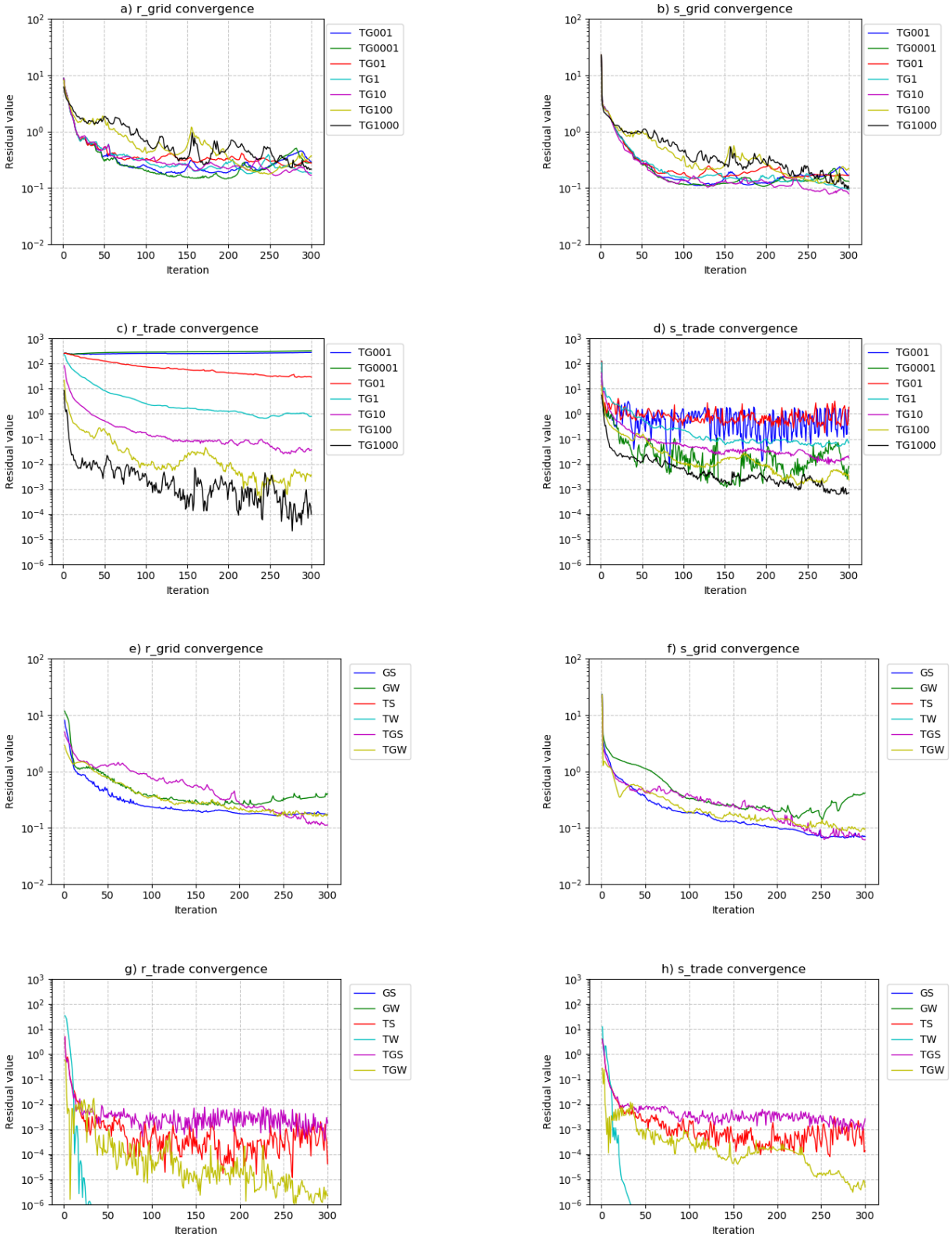

Figure 6: Convergence comparison for all scenarios. Figures a)-d) show comparison of residuals for scenarios 1-7, which are run for 1 day. Figures e)-h) show comparison of residuals for scenarios 8-15, which are run for 1 week. The residual values are combined for all households in the community. Note that e) and f) do not include results for TW and TS since only grid residuals are evaluated. Likewise, for figures g) and h), GW and GW are not shown.

Figure 7: Energy flows for day 1 of the week. All energy flows represent the combined total sum of all households in the community.

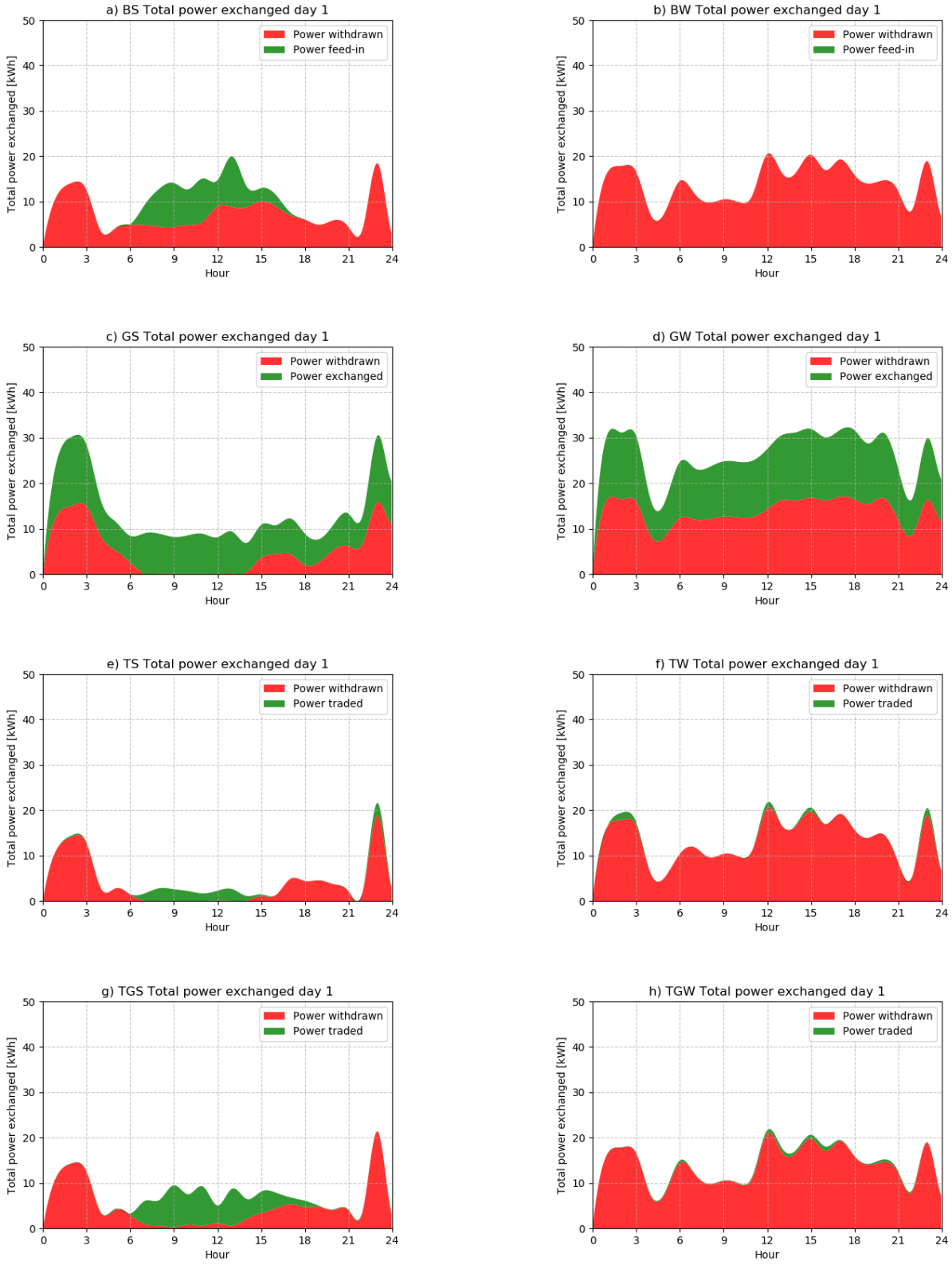

Figure 8: Total power exchanged for day 1 of the week. The total power exchanged represents the combined total sum of all households in the community. The green plot is stacked on top of the red plot. Note that in the baseline scenarios the green plot represents the feed-in power, in the grid-only scenarios it represents power exchanged (without trade price) and in the trade-only and combined scenarios it represents total volume of power traded.

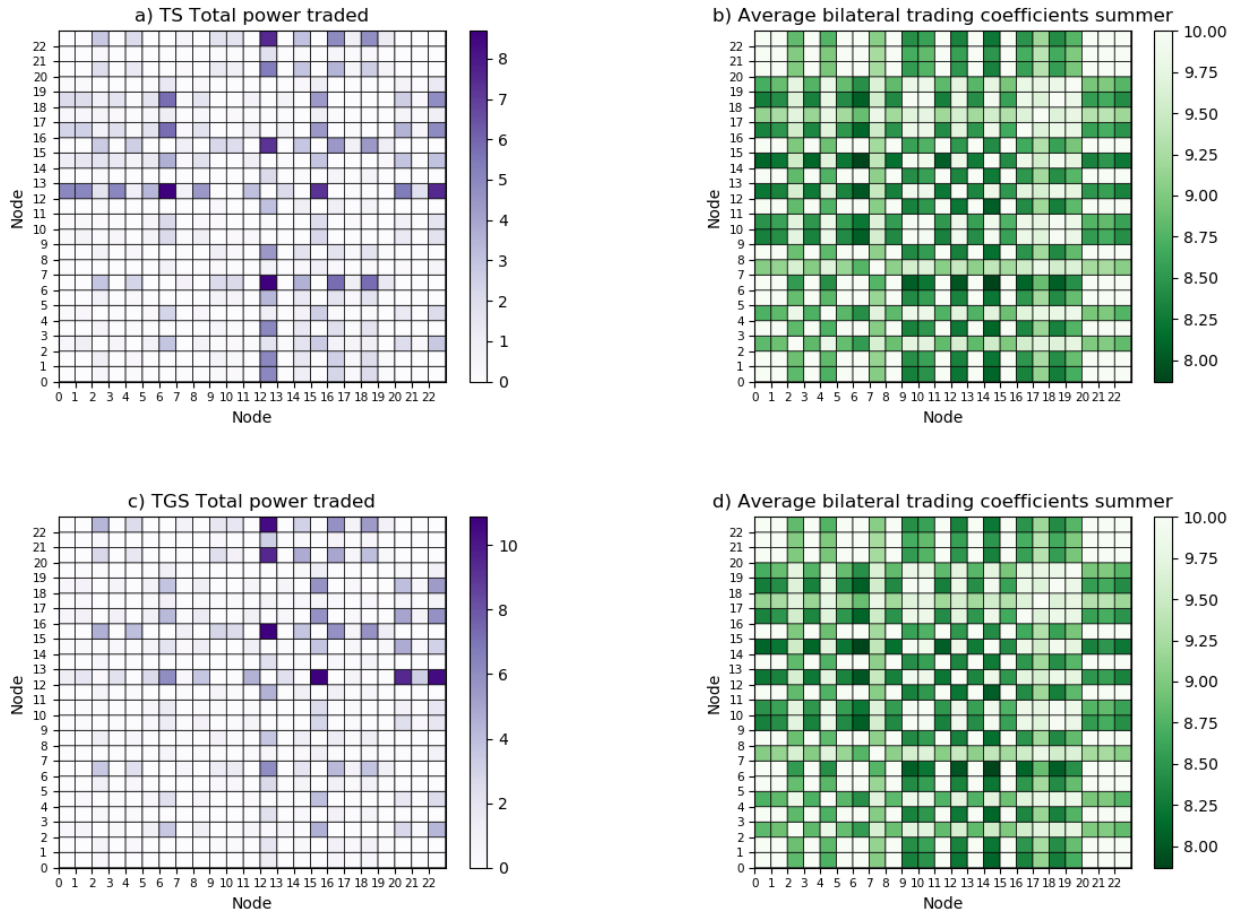

Figure 9: Sum of total power traded over the entire week between the nodes for the summer scenarios. A comparison is made with the bilateral trading coefficients, which are averaged over all timesteps of the entire week.

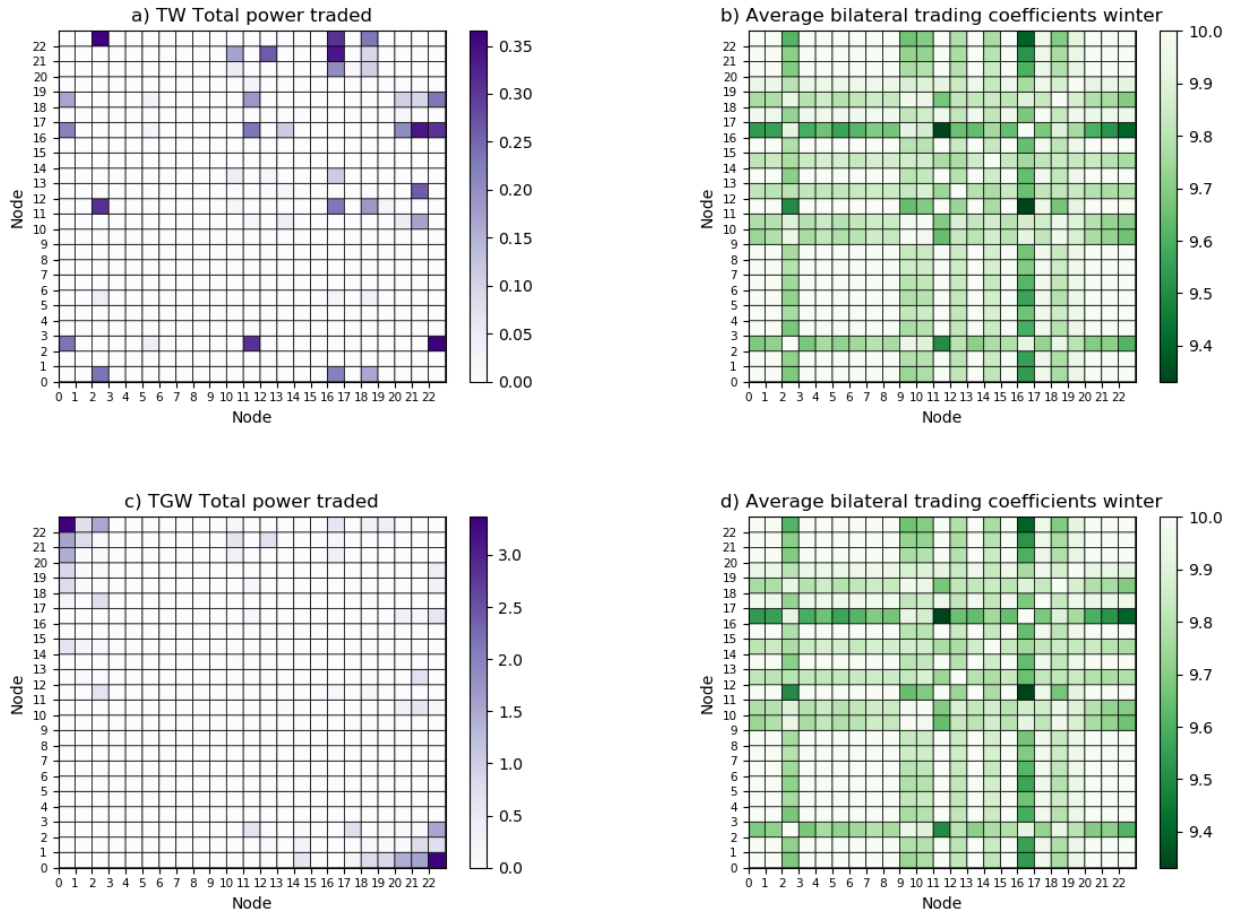

Figure 10: Sum of total power traded over the entire week between the nodes for the winter scenarios. A comparison is made with the bilateral trading coefficients, which are averaged over all timesteps of the entire week.

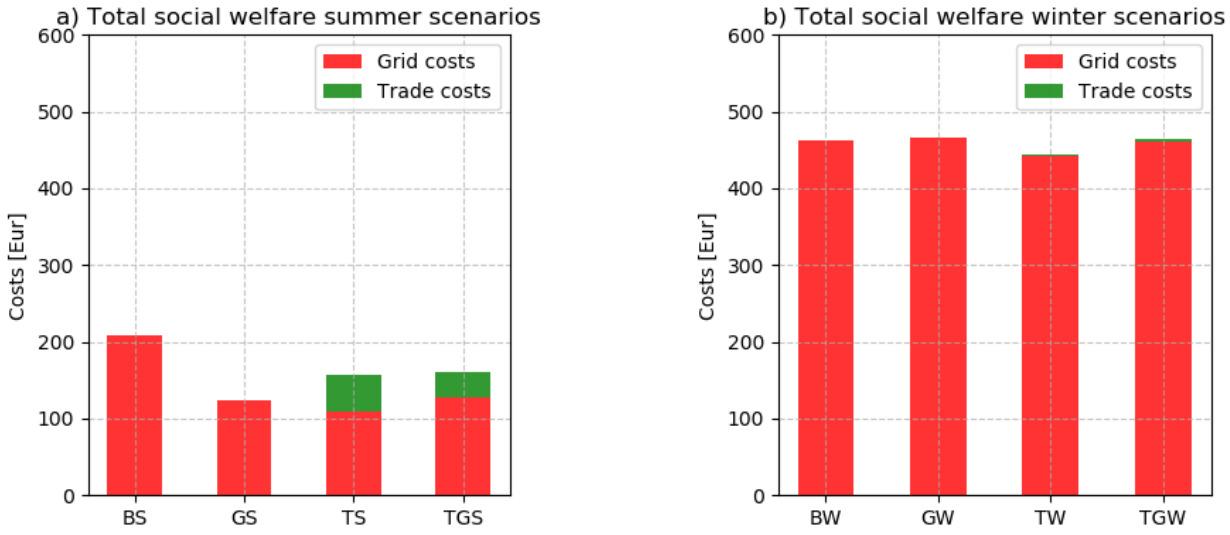

Figure 11: Social welfare comparison for all scenarios. The bars represent the total combined costs for all households over the entire week, with the green plot being stacked on top of the red plot. Note that the baseline and grid-only scenarios do not include trading costs.

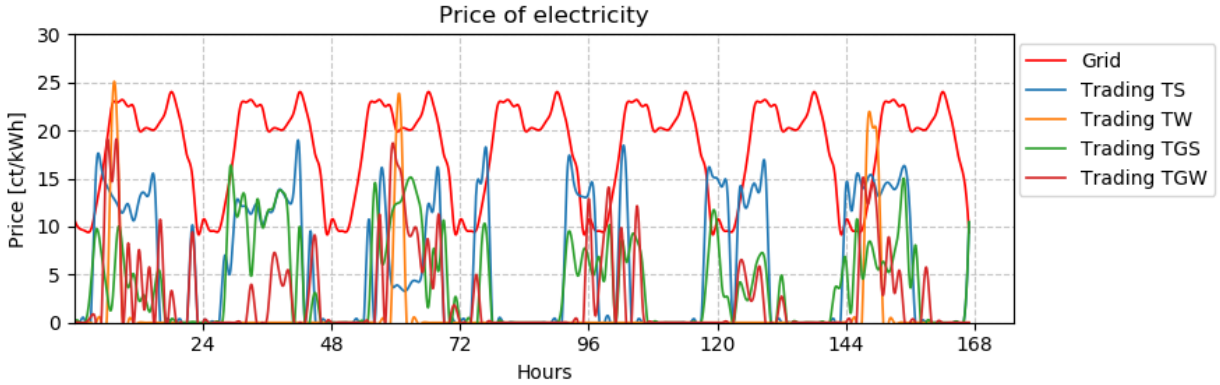

Figure 12: Price of electricity throughout the week for all scenarios. The bright red plot represents the costs of electricity from the grid, whereas the other plots represent the average price of trading across the whole community in every timestep.

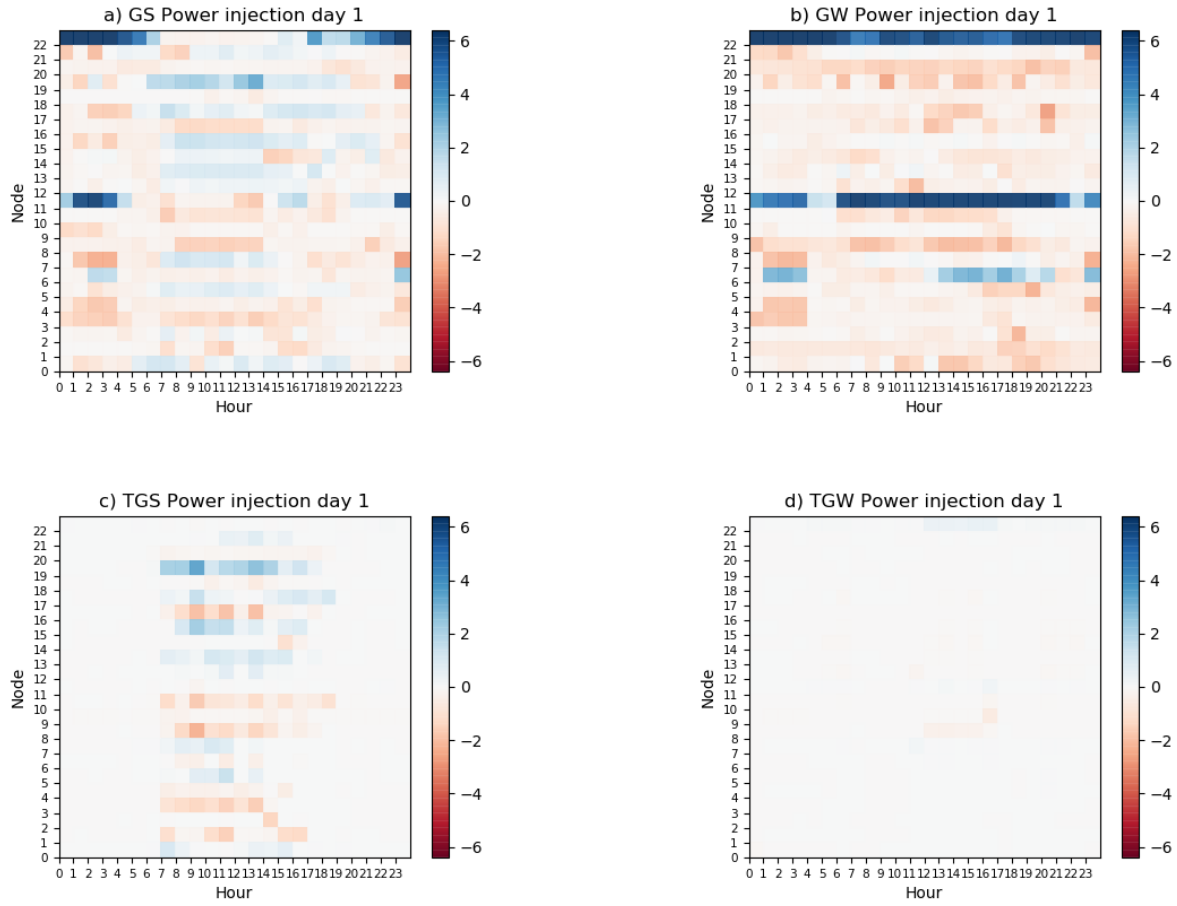

Figure 13: Power injection for day 1 for day one. Power injections into the microgrid are shown for every node in every timestep.

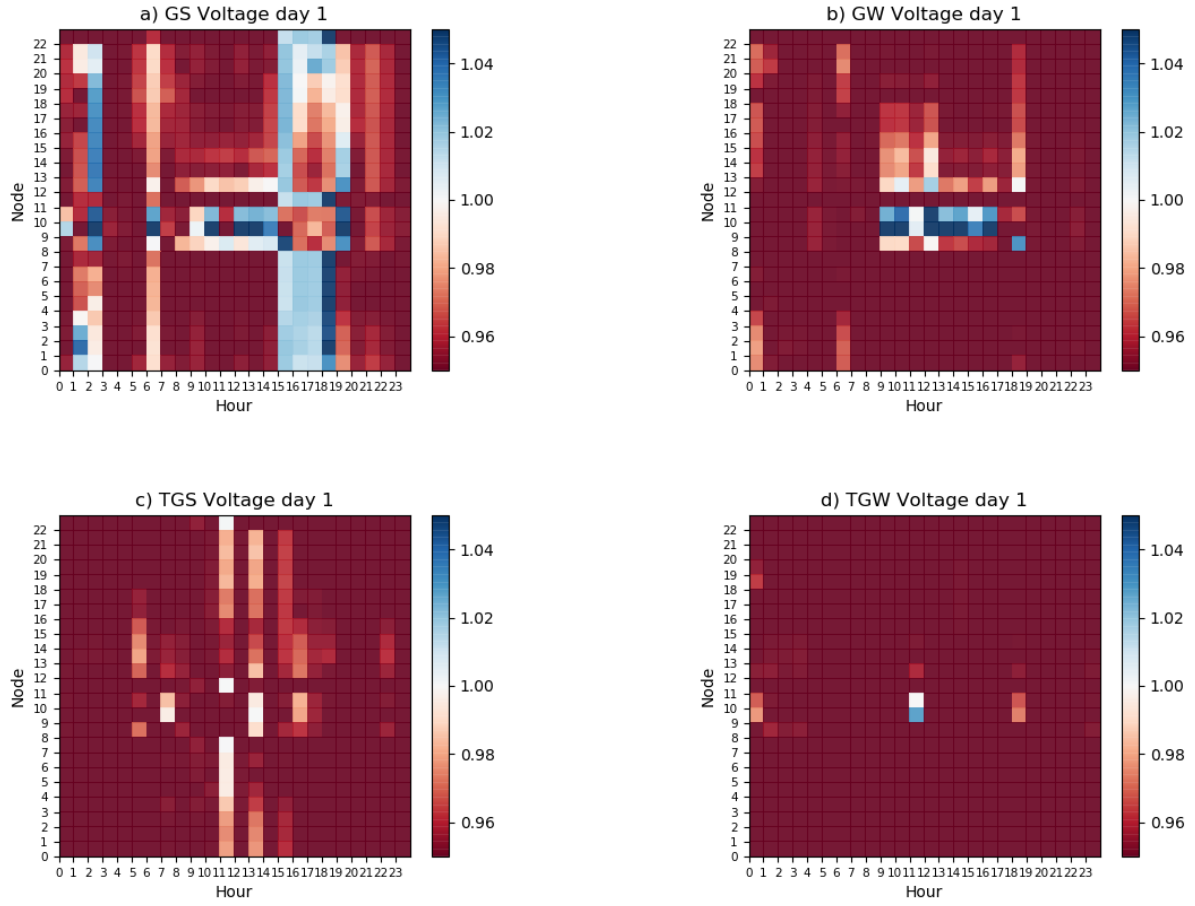

Figure 14: Voltage levels for all nodes for day 1 of the week.

4 Discussion

4.1 Interpreting the results

Based on the plots in Figure 6 the convergence of the ADMM algorithm can be compared for the different scenarios. For scenarios 1-7, results are similar for the residuals of the grid constraints portion of the model. Residuals decrease sharply in the first hundred iterations, after which convergence slows down considerably around values of 0.1. It can be seen that high values of ϕ, especially 100 and 1000, yield a stronger oscillation of convergence as well as a slower decrease of residuals initially. After 300 iterations however, residuals are around the same values as the other scenarios, and even a little bit lower. When looking at the trade residuals r_t and s_t, the difference between the scenarios becomes much clearer. For the r_t residual it can be seen that the model does not converge at all for ϕ values of below 1. Convergence accuracy increases significantly with the ϕ value. For s_t similar results can be seen, where only ϕ values of 100 and 1000 yield acceptable convergence of the algorithm. This can be explained by the $\phi/2$ factor in 30. As ϕ increases, the factor following $\phi/2$ is multiplied by a higher number, resulting in a larger need to reduce it in the following iteration. Since this factor contains the consensus constraint, a better convergence is achieved for higher values of ϕ. For low ϕ values of 0.001 and 0.01, the consensus factor is diminished in magnitude, reducing the need to enforce consensus by reducing the factor. For these reasons, a ϕ value of 1000 is chosen for scenarios 8-15.

For grid convergence of scenarios 8-15 it can be seen that convergence is very similar for all scenarios. Residual values sit below 10^{-1} for all scenarios after 300 iterations and appear to still be on a descending slope. For the present study, residual values of around 10^{-1} are considered acceptable for further analysis of the results considering that the values are calculated across over 10000 variables. The trade residuals of scenarios 1-15 show that by far the best convergence is achieved in the winter scenarios, which makes sense considering that it becomes much easier to find the optimal trading scheme and reach consensus in absence of excess PV generation. It can also be seen that addition of grid constraints (i.e. scenarios TGS and TGW) to the trading scenarios (i.e. scenarios TS and TW) results in a slower convergence for both winter and summer scenarios, but also for these scenarios residual values are well within acceptable limits, with the TGS scenario converging slowest around values of 10^{-3} after 300 iterations.

Figure 7 shows the scheduling of a number of energy flows on the first day for all scenarios. Overall, similar patterns can be recognized for all scenarios in summer as well as for all in winter. In the summer scenarios, it can be seen that grid withdrawals are highest during the nighttime hours. Peaks are seen around 11pm and 2am when the cost of electricity is low. It appears these withdrawals are primarily used to charge EVs and batteries, which show consumption peaks during the same hours. Grid withdrawals during the day are very low, except for the BS scenario where no excess PV power can be exchanged internally. Furthermore, it can be recognized that the TS and TGS scenarios yield higher withdrawals during evening peak hours than the GS scenario. Regarding the use of the battery systems, it can be recognized that the battery is charged during the day when there is excess PV power and during the night when electricity from the grid is cheap. Batteries are discharged during morning and evening peak hours to cover demand across the grid, reducing the amount of power that must be withdrawn externally. It can be seen that the GS scenario yields a larger use of battery systems, with higher peaks across the day, especially during peak hours and at nighttime around 3am. An increased use of battery systems means that the batteries will discharge and charge more often, resulting in a reduced lifetime. For households that have already invested into these battery systems, the reduced lifetime may incur extra costs in maintenance or replacement of the system. Since in the GS scenario the batteries are used for the balancing of power in the whole microgrid as well as increasing of overall welfare for the whole community, it may be unfair and undesirable to incur extra costs for these households. It appears that the inclusion of the trading mechanism inhibits excessive trading of battery energy during peak hours, which reduces overall use of the battery across the day. This is because during peak hours the electricity price is likely to be higher as demand is high and PV generation is relatively low. Overall, besides the BS scenario, the largest difference can be seen between the GS and other scenarios. Scheduling is very similar between the TS and TGS scenarios. For the winter scenarios it can be seen that all scenarios yield very similar patterns for the scheduling of energy flows. Since there is almost no PV generation there is very little excess power available, which makes the optimal solution look similar in all scenarios.

Figure 8 shows the amount of power withdrawn from the external grid as well as the excess budget of power that is either fed into the external grid, exchanged for free or traded between the households. In the summer scenarios, it can be seen that power withdrawn is by far highest for the baseline scenario, especially during the day. For the BS, TS and TGS scenarios it can be seen that the excess budget is traded or fed-in during

the day when there is an excess of PV generated power. Interestingly, the GS scenario shows a considerable amount of power being exchanged throughout the day and night, not just when there is solar. Without a price on trading there is no inhibition on exchanging power, and the increased battery activity observed in Figure 6 is also related to this increased exchange of power. When comparing the TS and TGS scenarios, it can be observed that there is significantly more power traded with the inclusion of grid constraints. It appears that this increased injection into the microgrid is necessary to respect these grid constraints. For example, the presence of reactive power flows throughout the microgrid could be related. Although all households have a small reactive power demand, reactive power can only be generated by owners of PV. As such, consumers are dependent on the injection of reactive power in the microgrid by prosumers. When reactive power flows through the microgrid, the branch flow model requires that there is also a flow of real power, resulting in an increased trading volume. For the winter scenarios a similar pattern is seen, where again in the grid-only scenario GW a large amount of power is exchanged. In the other scenarios there is no exchange of power.

The amount of power exchanged in the GW scenario is too large to be covered by the excess solar budget which means that households must be withdrawing electricity externally to inject into the microgrid. The same thing appears to be happening during the night in the GS scenario, as battery discharge in Figure 7 is too small to cover the amount of energy that is traded. It appears that withdrawing electricity externally to inject into the microgrid is most financially efficient way of covering all demand. For the total quantity of power that is withdrawn from the grid, Table 3 and Table 4 show the numerical results for all scenarios, as well as the total quantity of withdrawals during peak hours. Peak hours are defined as 6-9am in the morning and 5-8pm in the evening. From Table 3 it can be seen that in summer, withdrawals are by far highest in the baseline scenario with a total withdrawal of 1231 kWh. The TS scenario has the lowest withdrawal at 60% of baseline, with 741 kWh. GS and TGS scenarios show withdrawals of 915 and 862 kWh respectively. As can be expected, the most energy is withdrawn when there is no possibility of exchanging energy. It can be recognized that inclusion of grid constraints increases the amount of energy is withdrawn, which can be explained by the efficiency losses that are included in the branch flow equations 10a - 10d. Besides these losses it seems plausible that further efficiency losses must be incurred in order to respect the grid constraints. For the external grid withdrawal during peak hours, it can be recognized that this is by far the lowest in the GS scenario at 41.7% of BS. Inclusion of the trading mechanism increases peak withdrawals, yielding 55.9% in the TS scenario and 63.4% in the TGS scenario. This is consistent with the earlier observation that there is an increased exchange of energy during peak hours in the GS scenario by more frequent battery usage, whereas this is inhibited by the trading price in TS and TGS scenarios. It is interesting to observe that while total withdrawals are higher in the GS scenario than in TS and TGS, peak withdrawals are lower. When looking at the values for the winter scenarios in Table 3, it can be recognized there is little difference between the scenarios. Although there is some small variation, it is not large enough to be significant.

Figures 9 and 10 show the total amount of power traded between households as compared to the average bilateral trading coefficients. The coefficients are averaged across all timesteps. By comparing the figures it can be seen whether households are actually conducting trades with their preferred partners. Looking at the results for the summer scenarios in Figure 9, it does appear that this is the case. In the TS scenario for instance, node 12 is trading large amounts of energy with 0, 1, 3, 6, 15, 20 and 22. Low trading coefficients are imposed on these trades. Other nodes that trade a lot are 6 and 16, 6 and 18, 15 and 16 and 15 and 18. These trades too have low average coefficients associated with them. A similar pattern is seen for the TGS scenario. From 10 it can be recognized that the TW scenario shows a pattern that is similar to the summer scenarios. For the TGW scenario however it can be recognized that by far the most power is traded between node 0 and node 22, even though there is a high bilateral trading coefficient associated with this trade. Since nodes 0 and 22 are at the head and tail of the radial network respectively it appears that with the inclusion of grid constraints and absence of solar PV, it is most efficient to inject power at one end of the network and have it flow all the way to the end, effectively forcing the two nodes to trade. Since the bilateral trading coefficients are significantly higher in winter than they are in summer, it appears that their influence on the final optimal solution is smaller than that of physical grid constraints. Still, it should be emphasized that the quantity of power that is traded in winter, with the absolute maximum being around 3 kWh, is much lower than in the summer scenarios, where total trade quantities of around 8 kWh are commonplace.

Figure 11 shows the total social welfare of the whole network for the different scenarios, with costs being split up into grid costs and trade costs. Tables 3 and 4 shows numerical values for social welfare. The grid costs represent costs that are spent by the community as a whole, whereas trade costs are only individual costs since payments are made towards other members of the community. It can be recognized that for the summer scenarios, total costs are lowest for the GS scenario, at 59.5% of BS. Total costs for TS and TGS

scenarios are at 75% and 77% of BS costs respectively, which means that a significant reduction in total costs compared to baseline is observed for all scenarios. The TS scenario has lowest grid costs, which makes sense considering the scenario also has the lowest withdrawals. When comparing TS and TGS scenarios, TS has lower grid costs but higher trade costs. Total social welfare is similar for both. For the winter scenarios it can be seen that there is very little variation between the scenarios, which can again be explained by the absence of surplus solar PV power. In Tables 3 and 4, a comparison is also made between the costs that are made for prosumers and consumers. In summer, it can be recognized that in the TS and TGS scenarios the prosumer households costs are much lower than the consumer households since the prosumers make a profit on the trading, whereas consumers do not. The TS scenario shows 11.8% for prosumer costs compared to BS, and TGS shows 28.9%. Consumer costs for these scenarios are at 99.5% and 100% of baseline respectively. As such, it appears this effect is stronger without the inclusion of grid constraints. An interesting result is found in the GS scenario, where almost all costs of grid withdrawals are made by consumer households as opposed to prosumer households. In fact, prosumer costs are so low as to suggest that consumers withdraw from the external grid and feed it into the microgrid to deliver to the prosumers. Prosumer grid costs are 8% of baseline, whereas consumer grid costs are 119.7% of baseline. In the scenarios that include trading, the difference between prosumers and consumers is much smaller for the grid costs, and the differences only arise from the trading.

Figure 12 shows the variation of the price of electricity throughout week and compares the price of grid electricity with the price of trading of the different scenarios. It can be recognized that the price of trading is almost always lower than the price of external grid withdrawals, financially incentivizing internal trading. When looking at the summer scenarios, being the blue (TS) and green (TGS) plots, it can be seen that overall the TGS scenario yields a lower trading price than the TS scenario. When comparing the winter scenarios TW and TGW a similar pattern cannot be distinguished. However, the volume of trading in winter is so low that these results on the electricity price are relatively meaningless.

Figure 13 shows the power injection into the microgrid at the different nodes during the first day. Positive values represent injection whereas negative values represent withdrawal. Looking at the GS scenario, different patterns can be recognized during daytime and nighttime hours. During daytime, when there is an excess of PV electricity, it can be seen that injections are made at prosumer nodes like 19, 17, 15, 7 and 5. The consumer nodes are making withdrawals at these hours, as is to be expected. At the nighttime however, power injections are focused at two nodes, being node 11 and node 22. It can be seen that these injections approach the external grid withdrawal limit of 6.5kW. All other nodes make withdrawals from the microgrid at these times. Looking at the grid topology in Figure 5 it can be seen that node 22 is at the end of the radial network whereas node 11 is exactly halfway. It appears that in the absence of excess PV power, it is most efficient to inject large amounts of power through a single injection point to reduce the losses. The fact that there is still injection at all during these hours can be explained by the need respecting physical grid constraints. Looking at the GW scenario, where excess solar PV is almost non-existent, this pattern can be recognized even more clearly. Looking at the TGS and TGW scenario, it can be seen that inclusion of the trading mechanism prevents this injection into the grid when there is no excess PV. Figure 14 shows the voltage levels throughout the first day of the week at all nodes. It can be seen that at most times, at most nodes, voltage is at the minimum level of 0.95 of the nominal value. In the GS scenario, voltage fluctuations are highest. Voltage levels strongly increase during the night around 1-3am and in the afternoon around 3-7pm. In the night, the voltage increase appears to be related to the high injections in nodes 22 and 11 at times when consumption is low. In the afternoon, the high voltage levels seem to coincide with times of high consumption and moderate PV generation, i.e. peak hours. Still, it can be seen that minimum and maximum limits are respected at all times. In the GW scenario, there is an increase in voltage in the nodes 8-13 during the daytime hours of 9-4pm. This could be related to the large injections that are made at node 11. Still, voltage levels are again well within limits. In the TGS scenario, small fluctuations in voltage levels can be seen during the daytime hours when there is an excess of PV power that is fed into the grid.

4.2 Comparing the scenarios

When comparing the scenarios with all results taken into consideration, some general patterns emerge. First of all, convergence of ADMM for all scenarios is similar and sufficient for the present purposes. Convergence is slower when combining trade and grid constraints, which is to be expected given the increase in complexity of the optimization problem. Furthermore, it can be recognized that for the winter week the results of the different scenarios show little variation across all categories. It appears that the impact of implementing a platform such as the one proposed emerges in presence of a considerable excess of PV power. Therefore,

further comparison is focused on the results from the summer scenarios.

First of all, the BS scenario represents a situation that is similar to the present organization in the distribution grid. There is no cooperation between households on any level, and prosumers may dispose of their excess PV-generated electricity by feeding it into the grid. A financial compensation is offered to them in the form of FiT, and battery storage systems are only for private use. Consumers are completely reliant on their energy service providers to provide them with affordable, reliable and clean energy as is desired. Also, this scenario requires the DSO to optimally redistribute energy in the grid and ensure that all physical constraints are respected. Given the expected increase in DER adoption [8] [66], this task will become more and more complex. Furthermore, considering the expected abolishment of FiT [10], prosumers must find other ways to optimally benefit from their installed PV systems. Coupled with the rise of P2P markets, the increased desire for independence and free choice, and other developments discussed in section 1.1, it seems likely that the system configuration represented in the baseline scenarios will increasingly be replaced by other types of systems. This is reinforced by the result from this study that the BS scenario yields the highest total costs and external grid withdrawals of all summer scenarios.

Out of the GS, TS and TGS scenarios, the GS scenario shows favourable results for total social welfare. Total costs in this scenario are at 59% of baseline considerably lower than for the other scenarios, which means that total social welfare is the highest. However, the scenario also has the highest grid withdrawals at 74% of baseline. Since peak withdrawals are lowest, it appears that this scenario makes optimal use of the cheap electricity during non-peak hours. This could be beneficial for the DSO and the external grid as a whole as congestion might be reduced, as well as the need for the dispatch of flexible fossil fuel generation during these peak hours. There are some downsides too however. First of all, a larger and more frequent use of battery systems is required. This may incur extra costs in maintenance and possible replacement of battery systems for their respective owners. These costs are not included in the model. Furthermore, there is a large inequality between prosumer costs and consumer costs, even without the prosumer market power that comes with the trading mechanism. This inequality emerges from the large withdrawals made by nodes 22 and 11 during the nighttime: both of these nodes happen to be consumer households. It appears that these nodes make the largest withdrawals not because they are consumers, but because they are a located at the end point and halfway point of the radial grid. When considering physical constraints, it is most efficient to inject large quantities of power at these locations rather than to inject small quantities at many different nodes. Since the objective is to minimize total costs of the community as a whole, the algorithm does not consider inequalities in the individual costs made by the different households. Because of this, the GS scenario appears to only be viable when costs of grid withdrawals are fairly shared across all members of the network. Furthermore, a way must be found to compensate owners of PV and batteries for their extra contribution to the total welfare of the community. This would require intensive cooperation between all participants on the network, and the resulting community would be akin to an energy collective as discussed in section 1.2. In such a community, there would be no need for a trading mechanism since all households will act in the interest of the group.

When intensive cooperation is not possible and households act in a self-interested manner however, the inclusion of a trading mechanism can regulate this whilst still ensuring maximization of total social welfare. In the TS and TGS scenarios the large injections made at nodes 11 and 22 are not observed. When comparing the TS and TGS scenarios, costs of grid withdrawals are very similar for prosumers and consumers, and inequality in costs made only emerge from trading. Inequality is larger in the TS scenario and more money is exchanged through trading. Interestingly, the quantity of energy traded is actually lower in the TS scenario, whereas the internal price of trading electricity is higher. This means that the prosumers have a larger market power in the TS scenario which drives up the price of electricity and inhibits further buying by consumers. The TS scenario seems viable when all participants on the network are primarily self-interested and little cooperation between them is possible or desirable. Such a network may be akin to a full P2P market as discussed in section 1.2. The mechanism allows prosumers to benefit maximally from their PV and battery systems, and the bilateral trading coefficients are guaranteed to be respected at all times, whereas including grid constraints may prevent this as has been observed in the TGW scenario. Furthermore, grid management is left to the DSO, resulting in reduced energy use and costs within the community, as can be observed when comparing the TS and TGS scenarios. In fact, total grid withdrawal is lowest for the TS scenario at 60% of baseline. In the TGS scenario, the lower price on internal trades means that market power of prosumers is reduces by the introduction of physical constraints. This can be explained by the fact that the model requires that power is injected in order to respect the grid constraints. This required injection by prosumers can be seen as an extra contribution to total social welfare as the task of balancing the grid

is taken over from the DSO at the cost of extra profit. Even though total costs and energy consumption are slightly higher in the TGS scenario than in the TS scenario, the extra costs and efficiency losses are simply moved from the community to the DSO in the TS scenario. In the TGS scenario, the community basically takes responsibility for the managing of its local electricity infrastructure, which fits the idea of independence and free choice. Of course, there would still have to be cooperation between the community and the DSO regarding maintenance of the grid, and it seems plausible that financial compensation could be offered by the DSO to the community or its individual members for their contribution to grid management. It is interesting to observe that the adoption of responsibility for grid balancing in the TGS scenario results in reduced inequality between households. Also, when comparing TGS to GS, it is observed that inclusion of the trading mechanism actually reduces total external grid withdrawals, making it the more environmentally friendly option.

When considering the research questions 1a, 1b and 1c, there are some answers that can be given to answer these questions. For the convergence of ADMM, it appears from the present study that it is not too strongly affected by the combination of physical constraints and market mechanism. Although convergence is somewhat slower in the combined scenarios, it is still at an acceptable level. For social welfare, it appears that the best result is achieved without implementing a trading mechanism, and a combination of grid constraints and trading mechanism yields lowest social welfare. However, when considering only grid constraints a strong inequality of social welfare within the community arises as all costs of grid withdrawals are made by only a couple of households. When considering only trading, there is also a large inequality in social welfare as the market power of prosumers is unbounded. This allows them to sell electricity to consumers for higher prices. When combining trading and grid constraints, both these inequality effects are mitigated, resulting in a more balanced end result. In this combined scenario, total costs are reduced by 23% compared to the baseline scenario, and total electricity withdrawal is reduced by 30%. Also, it is more environmentally friendly than the GS scenario, and possibly even than the TS scenario depending on the efficiency losses incurred by the DSO grid management. Overall, it seems that applicability of the different scenarios in real life is dependent on the nature of the cooperation between the participants, as well as the cooperation between the community and the DSO. Given that the present study proposes a platform that is implemented on blockchain, it seems reasonable that adopters of such platforms hold independence, free choice and anonymity in high regard, which could make it feasible or them to adopt any of the platforms modelled in the different scenarios. A platform similar to the GS scenario would fit a situation where independence and welfare of the community as a whole are deemed imporant. In this case, individuals must be prepared to collaborate intensively to fairly share costs and take responsibility for grid management. The TS scenario seems to fit a community where participants prioritize individual choice, freedom and welfare and do no desire to be involved in local grid management. The TGS scenario represents a middle ground where extra responsibility is adopted for management of the grid, but where cooperation between participants is regulated by a trading mechanism.

4.3 Limitations of the model

Although conclusions can be drawn from the present study, there are several limitations that should be considered. First of all, the modelled platform is intended to function as a day-ahead optimization platform, meaning that outcomes are dependent on accuracy of generation and consumption forecasts. Regarding the implementation on blockchain, the suggested configuration has not been extensively tested for communication efficiency, security and execution speed, even though these are important factors. The aim of this study has been to provide a general framework for implementation and for using the smart contract. Regarding the development of the model, there are always inherent uncertainties in the software that is used, in this case Python, Cvxpy, Ganache-cli and Web3.py. Also, uncertainties are inherently present in the branch flow model and the ADMM algorithm, since a distributed algorithm will never converge to exactly the same solution as a centralized algorithm. Other important limitations arise from the assumptions that are made in the setup of the model. It has been assumed that all EVs have the same average charging demand and charging hours every day, which is not likely to occur in a real-life situation. Also, values have been assumed for the battery parameters, and assumptions have been made regarding the availability of reactive power generation and the topology of the grid. It is unclear whether varying the amount or distribution of DER in the grid will severely affect the outcome, and the investment costs of the various assets has not been taken into account. For battery systems in particular, the investment costs can play a large role when making financial calculations in a model. Finally, the bilateral trading coefficients may have large impacts on the outcomes of the model. In this study, an effort has been made to set realistic values for the bilateral trading coefficients in a relatively straightforward manner, but a more extensive modelling of prosumer market behaviour may

provide further insights into the impact of the coefficient values.

5 Conclusion

This study has shown the modelling of an integrated blockchain-based energy management platform that respects physical grid constraints and implements a bilateral trading mechanism. The procedure of integrating the physical, economic and information layers in a single model has been shown in section 2. As a first main contribution, the formulation of a distributed optimization problem that respects physical grid limitations through OPF and implements a bilateral trading mechanism has been detailed in section 2.4. As a second main contribution, the implementation of the distributed algorithm on a blockchain network has been specified in section 2.5. In order to answer research question 2), it is detailed in this section how a smart contract can take on the role of virtual aggregator. It has been shown that there are several important functions that the smart contract has to fulfill: Not only does it have to execute the consensus step from the ADMM algorithm, it also functions as a central agent for distributing required information and data to all other nodes and it ensures that the algorithm is executed symmetrically by all nodes. In order to answer research question 1), performance and outcomes of the proposed model are evaluated by running several scenarios, the setup of which has been detailed in section 2.6. The results of running the scenarios have been shown in section 3 and have been discussed in section 4. It has been shown that the ADMM algorithm performs well with the combined optimization problem and achieves acceptable convergence. Furthermore, although combining the trading mechanism and physical constraints yield a somewhat lower total social welfare, inequality between households in the community is reduced as compared to the trade-only and grid-only scenarios. This is because the trading mechanism prevents few households from withdrawing all power to supply the whole community, and the physical constraints reduce the prosumer market power. As such, it appears that there are considerable benefits to combining trading with grid constraints when designing energy optimization platforms, especially when comparing to the baseline scenario: Costs are reduced by 23% and total energy use is reduced by 30% as compared to the status-quo. Still, the practical applicability of the different scenarios in real life depends on the needs and priorities of the participants. It is argued that the combined that a trade-only scenario could represent full P2P type markets, whereas a grid-only scenario could represent an energy collective. The combined scenario could represent a middle-ground where several downsides of the other scenarios are mitigated. Research into the social acceptance of the different scenarios and actual wishes of participants could give further insights into the practical feasibility. The usefulness of the proposed model can be expanded in several ways. First of all, the model could be implemented on a real blockchain network to evaluate security, efficiency and execution speed in a real life situation. Furthermore, the sensitivity of modelling results to input parameters such as trading coefficients, investment costs and DER distribution could be explored. Also, a detailed techno-economic assessment could be carried out to evaluate social welfare over an extended period of time.

References

[1] J. Rogelj, M. Den Elzen, N. Höhne, T. Fransen, H. Fekete, H. Winkler, R. Schaeffer, F. Sha, K. Riahi, and M. Meinshausen, "Paris Agreement climate proposals need a boost to keep warming well below 2 c," *Nature*, vol. 534, no. 7609, pp. 631–639, 2016.

[2] S. Chu, Y. Cui, and N. Liu, "The path towards sustainable energy," *Nature Materials*, vol. 16, no. 1, pp. 16–22, 2016. [Online]. Available: http://dx.doi.org/10.1038/nmat4834

[3] A. Baranzini, J. C. van den Bergh, S. Carattini, R. B. Howarth, E. Padilla, and J. Roca, "Carbon pricing in climate policy: seven reasons, complementary instruments, and political economy considerations," *Wiley Interdisciplinary Reviews: Climate Change*, vol. 8, no. 4, pp. 1–17, 2017.

[4] M. Nicolini and M. Tavoni, "Are renewable energy subsidies effective? Evidence from Europe," *Renewable and Sustainable Energy Reviews*, vol. 74, no. July 2016, pp. 412–423, 2017. [Online]. Available: http://dx.doi.org/10.1016/j.rser.2016.12.032

[5] B. Bakhtyar, A. Fudholi, K. Hassan, M. Azam, C. H. Lim, N. W. Chan, and K. Sopian, "Review of CO2 price in Europe using feed-in tariff rates," *Renewable and Sustainable Energy Reviews*, vol. 69, no. October 2015, pp. 685–691, 2017. [Online]. Available: http://dx.doi.org/10.1016/j.rser.2016.11.146

[6] E. Kabir, P. Kumar, S. Kumar, A. A. Adelodun, and K. H. Kim, "Solar energy: Potential and future prospects," *Renewable and Sustainable Energy Reviews*, vol. 82, no. August 2017, pp. 894–900, 2018.

[7] A. Ipakchi and F. Albuyeh, "Grid of the future," *IEEE Power Energy Magazine*, vol. 7, no. 2, pp. 52–62, 2009.

[8] H. Farhangi, "Path of the smart grid," *IEEE Power and Energy Magazine*, vol. 8, no. 1, pp. 18–28, 2010.

[9] EURELECTRIC, "Prosumers â an integral part of the power system and the market," *Eurelectric*, no. June, p. 15, 2015. [Online]. Available: http://www.eurelectric.org/media/178736/prosumers_an-integral_part_of_the_power_system_and_market_june_2015-2015-2110-0004-01-e.pdf

[10] G. of the Netherlands, "Salderingsregeling verlengd tot 2023," 2019. [Online]. Available: https://www.rijksoverheid.nl/actueel/nieuws/2019/04/26/salderingsregeling-verlengd-tot-2023

[11] J. Driesen and F. Katiraei, "Design for distributed energy resources," *IEEE Power Energy Magazine*, vol. 6, no. 3, pp. 30–39, 2008.

[12] T. AlSkaif, A. C. Luna, M. G. Zapata, J. M. Guerrero, and B. Bellalta, "Reputation-based joint scheduling of households appliances and storage in a microgrid with a shared battery," *Energy and Buildings*, vol. 138, pp. 228–239, 2017. [Online]. Available: http://dx.doi.org/10.1016/j.enbuild.2016.12.050

[13] P. Pinson, T. Baroche, F. Moret, T. Sousa, E. Sorin, and S. You, "The Emergence of Consumer-centric Electricity Markets," *Distribution and Utilitization*, pp. 1–5, 2017. [Online]. Available: http://pierrepinson.com/docs/pinsonetal17consumercentric.pdf

[14] C. Giotitsas, A. Pazaitis, and V. Kostakis, "A peer-to-peer approach to energy production," *Technology in Society*, vol. 42, pp. 28–38, 2015. [Online]. Available: http://dx.doi.org/10.1016/j.techsoc.2015.02.002

[15] L. Einav, C. Farronato, and J. Levin, "Peer-to-Peer Markets," 2016.

[16] C. Zhang, J. Wu, C. Long, and M. Cheng, *IEEE Transactions on Smart Grid*, no. 3, pp. 1439–1450.

[17] T. Van Der Schoor and B. Scholtens, "Power to the people: Local community initiatives and the transition to sustainable energy," *Renewable and Sustainable Energy Reviews*, vol. 43, pp. 666–675, 2015. [Online]. Available: http://dx.doi.org/10.1016/j.rser.2014.10.089

[18] T. Sousa, T. Soares, P. Pinson, F. Moret, T. Baroche, and E. Sorin, "Peer-to-peer and community-based markets: A comprehensive review," pp. 367–378, 2019. [Online]. Available: https://doi.org/10.1016/j.rser.2019.01.036

[19] S. Kakran and C. Saurabh, "Smart operations of smart grids integrated with distributed generation: A review," *Renewable and Sustainable Energy Reviews*, vol. 81, pp. 524–535, 2018.

[20] Z. Ma, J. Xie, H. Li, Q. Sun, Z. Si, J. Zhang, and J. Guo, "The role of data analysis in the development of intelligent energy networks," *IEEE Network*, vol. 31, no. 5, pp. 88–95, 2017.

[21] T. AlSkaif, I. Lampropoulos, M. van den Broek, and W. van Sark, "Gamification-based framework for engagement of residential customers in energy applications," *Energy Research and Social Science*, vol. 44, no. May, pp. 187–195, 2018. [Online]. Available: https://doi.org/10.1016/j.erss.2018.04.043

[22] M. A. A. Pedrasa, T. D. Spooner, and I. F. MacGill, "Coordinated scheduling of residential distributed energy resources to optimize smart home energy services," *IEEE Transactions on Smart Grid*, vol. 1, no. 2, pp. 134–143, 2010.

[23] M. Andoni, V. Robu, D. Flynn, S. Abram, D. Geach, D. Jenkins, P. McCallum, and A. Peacock, "Blockchain technology in the energy sector: A systematic review of challenges and opportunities," pp. 143–174, 2019. [Online]. Available: https://doi.org/10.1016/j.rser.2018.10.014

[24] J. Yli-Huumo, K. Deokyoon, S. Choi, S. park, and K. Smolander, "Where is current research on blockchain technology? - a systematic review," *PLoS ONE*, vol. 10, no. 11, 2016.

[25] S. Nakamoto, "Bitcoin," 2019. [Online]. Available: https://bitcoin.org/bitcoin.pdf

[26] G. Wood, "Ethereum: a secure decentralised generalised transaction ledger," *Ethereum Project Yellow Paper*.

[27] D. Hammerstrom, S. Widergren, and C. Irwin, "Evaluating transactive systems," *IEEE Electrification Magazine*, 2016.

[28] M. H. Albadi and E. F. El-Saadany, "A summary of demand response in electricity markets," *Electric Power Systems Research*, vol. 78, no. 11, pp. 1989–1996, 2008.

[29] P. Siano, "Demand response and smart grids - A survey," *Renewable and Sustainable Energy Reviews*, vol. 30, pp. 461–478, 2014. [Online]. Available: http://dx.doi.org/10.1016/j.rser.2013.10.022

[30] G. Chen, F. L. Lewis, E. N. Feng, and Y. Song, "Distributed Optimal Active Power Control of Multiple Generation Systems," *IEEE Transactions on Industrial Electronics*, vol. 62, no. 11, pp. 7079–7090, 2015.

[31] Y. Wang, W. Saad, Z. Han, H. V. Poor, and T. BaÅar, "A game-theoretic approach to energy trading in the smart grid, url = https://doi.org/10.1016/j.apenergy.2018.03.010, volume = 5, year = 2014," *IEEE Transactions on Smart Grid*, no. 3, pp. 1439–1450.

[32] J. A. Taylor, *Convex Optimization of Power Systems*. Cambridge University Press, feb 2015. [Online]. Available: https://www.cambridge.org/core/product/identifier/9781139924672/type/book

[33] R. Carli and M. Dotoli, "A Decentralized Control Strategy for the Energy Management of Smart Homes with Renewable Energy Exchange," in *2018 IEEE Conference on Control Technology and Applications, CCTA 2018*, no. April. IEEE, 2018, pp. 1662–1667.

[34] A. Kargarian, J. Mohammadi, S. Member, J. Guo, S. Member, S. Chakrabarti, S. Member, M. Barati, G. Hug, S. Member, S. Kar, and R. Baldick, "Toward Distributed / Decentralized DC Optimal Power Flow Implementation in Future Electric Power Systems," *IEEE Transactions on Smart Grid*, vol. 9, no. 4, pp. 2574–2594, 2018.

[35] E. Münsing, J. Mather, and S. Moura, "Blockchains for decentralized optimization of energy resources in microgrid networks," in *Control Technology and Applications (CCTA), 2017 IEEE Conference on*. IEEE, 2017, pp. 2164–2171.

[36] J. Guerrero, A. C. Chapman, and G. Verbic, "Decentralized P2P Energy Trading under Network Constraints in a Low-Voltage Network," p. 1, 2018.

[37] M. Kraning, E. Chu, J. Lavaei, and S. Boyd, "Message Passing for Dynamic Network Energy Management," vol. 1, no. 2, pp. 70–122, 2012. [Online]. Available: http://arxiv.org/abs/1204.1106

[38] M. L. Di Silvestre, P. Gallo, M. G. Ippolito, E. R. Sanseverino, and G. Zizzo, "A technical approach to the energy blockchain in microgrids," *IEEE Transactions on Industrial Informatics*, vol. 14, no. 11, 2018.

[39] T. Morstyn, A. Teytelboym, and M. D. McCulloch, "Bilateral contract networks for peer-to-peer energy trading," *IEEE Transactions on Smart Grid*, vol. 10, no. 2, pp. 2026–2035, 2019.

[40] T. Morstyn and M. McCulloch, "Multi-Class Energy Management for Peer-to-Peer Energy Trading Driven by Prosumer Preferences," pp. 1–9, 2018.

[41] E. Mengelkamp, J. Gärttner, K. Rock, S. Kessler, L. Orsini, and C. Weinhardt, "Designing microgrid energy markets: A case study: The Brooklyn Microgrid," *Applied Energy*, vol. 210, pp. 870–880, 2018. [Online]. Available: https://doi.org/10.1016/j.apenergy.2017.06.054

[42] F. Moret and P. Pinson, "Energy Collectives: a Community and Fairness based Approach to Future Electricity Markets," *IEEE Transactions on Power Systems*, pp. 1–11, 2018.

[43] C. Long, J. Wu, Y. Zhou, and N. Jenkins, "Peer-to-peer energy sharing through a two-stage aggregated battery control in a community Microgrid," *Applied Energy*, vol. 226, no. May, pp. 261–276, 2018. [Online]. Available: https://doi.org/10.1016/j.apenergy.2018.05.097

[44] W. Tushar, T. K. Saha, C. Yuen, P. Liddell, R. Bean, and H. V. Poor, "Peer-to-Peer Energy Trading With Sustainable User Participation: A Game Theoretic Approach," *IEEE Access*, vol. 6, pp. 62 932–62 943, 2018.

[45] A. Lüth, J. M. Zepter, P. Crespo del Granado, and R. Egging, "Local electricity market designs for peer-to-peer trading: The role of battery flexibility," *Applied Energy*, vol. 229, no. May, pp. 1233–1243, 2018.

[46] T. Baroche, F. Moret, and P. Pinson, "Prosumer Markets: A Unified Formulation," in *IEEE PowerTech Conference*, 2019, pp. 1–6.

[47] I. Faber, W. Lane, W. Pak, M. Prakel, C. Rocha, and J. V. Farr, "Micro-energy markets: The role of a consumer preference pricing strategy on microgrid energy investment," *Energy*, vol. 74, no. C, pp. 567–575, 2014. [Online]. Available: http://dx.doi.org/10.1016/j.energy.2014.07.022

[48] E. Sorin, L. Bobo, and P. Pinson, "Consensus-Based Approach to Peer-to-Peer Electricity Markets with Product Differentiation," *IEEE Transactions on Power Systems*, vol. 34, no. 2, pp. 994–1004, 2019.

[49] Y. Wang, W. Saad, Z. Han, H. V. Poor, and T. BaÅar, "A game-theoretic approach to energy trading in the smart grid," *IEEE Transactions on Smart Grid*, vol. 5, no. 3, pp. 1439–1450, 2014. [Online]. Available: http://www.ncbi.nlm.nih.gov/pubmed/27695049{%}0Ahttp://www.pubmedcentral.nih.gov/articlerender.fcgi?artid=PMC5047482

[50] Z. Li, J. Kang, R. Yu, D. Ye, Q. Deng, and Y. Zhang, "Consortium blockchain for secure energy trading in industrial internet of things," *IEEE Transactions on Industrial Informatics*, vol. 14, no. 8, pp. 3690–3700, 2018.

[51] I. Lampropoulos, G. Vanalme, and W. Kling, "A methodology for modeling the behavior of electricity prosumers within the smart grid," 2010.

[52] C. Liu, K. K. Chai, X. Zhang, and Y. Chen, "Peer-to-peer electricity trading system: smart contracts based proof-of-benefit consensus protocol," *Wireless Networks*, vol. 0, 2019. [Online]. Available: https://doi.org/10.1007/s11276-019-01949-0http://link.springer.com/10.1007/s11276-019-01949-0

[53] S. Boyd, "Distributed Optimization and Statistical Learning via the Alternating Direction Method of Multipliers," *Foundations and Trends® in Machine Learning*, vol. 3, no. 1, pp. 1–122, 2011.

[54] T. Erseghe, "Distributed optimal power flow using ADMM," *IEEE Transactions on Power Systems*, vol. 29, no. 5, pp. 2370–2380, 2014.

[55] S. Adhikari and F. Li, "Coordinated v-f and p-q control of solar photovoltaic generators with mppt and battery storage in microgrids," *IEEE Transactions on Smart Grid*, vol. 5, no. 3, 2014.

[56] M. E. Baran and F. F. Wu, "Optimal capacitor placement on radial distribution systems," *IEEE Transactions on power Delivery*, vol. 4, no. 1, pp. 725–734, 1989.

[57] J. A. Taylor, *Convex optimization of power systems*. Cambridge University Press, 2015.

[58] Ethereum, "Web3.py," 2019. [Online]. Available: https://https://github.com/ethereum/web3.py

[59] S. Diamond and S. Boyd, "Cvxpy: A python-embedded modeling language for convex optimization," *The Journal of Machine Learning Research*, vol. 17, no. 1, pp. 2909–2913, 2016.

[60] TruffleSuite, "Ganache-cli," 2019. [Online]. Available: https://github.com/trufflesuite/ganache-cli

[61] EHPC, "East Harbour Prosumers Community platform for sustainable energy use," 2019. [Online]. Available: http://www.prosumers.nl/

[62] N. Li, L. Chen, and S. H. Low, "Exact convex relaxation of OPF for radial networks using branch flow model," in *2012 IEEE Third International Conference on Smart Grid Communications (SmartGridComm)*. IEEE, 2012, pp. 7–12.

[63] E. P. E. Netherlands, "Day-ahead auction," 2019. [Online]. Available: http://www.apxgroup.com/trading-clearing/day-ahead-auction/

[64] S. van der Stelt, T. AlSkaif, and W. van Sark, "Techno-economic analysis of household and community energy storage for residential prosumers with smart appliances," *Applied Energy*, vol. 208, 2018.

[65] CBS, "CBS StatLine - Verkeersprestaties personenauto's; kilometers, brandstofsoort, grondgebied," 2018. [Online]. Available: https://bit.ly/2OJtaCy

[66] J. Mayer, "Current and future cost of photovoltaics," 2015.

A Full week graphics

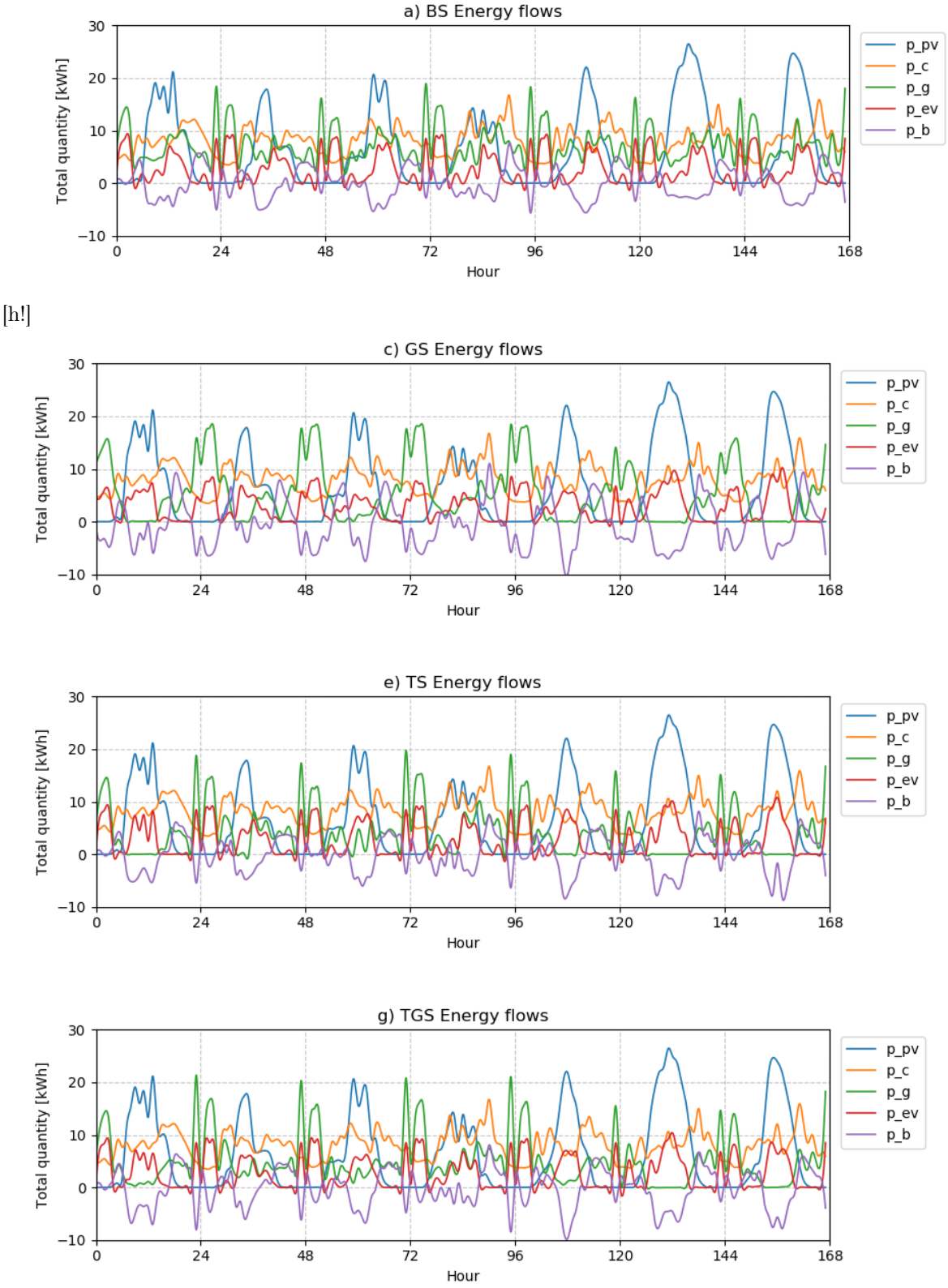

[h!]

Figure 15: Energy flows for summer scenarios

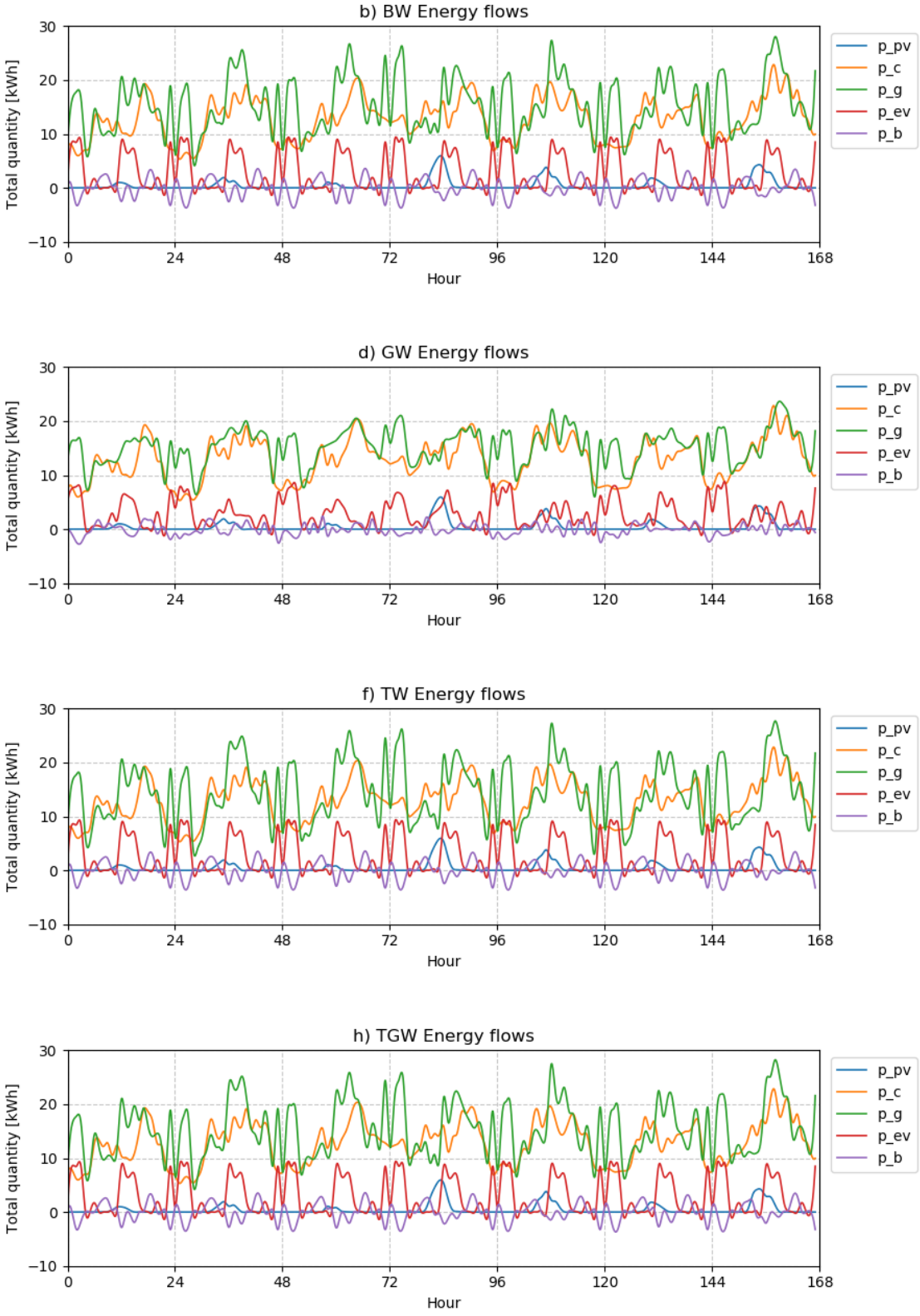

Figure 16: Power exchanged for winter scenarios

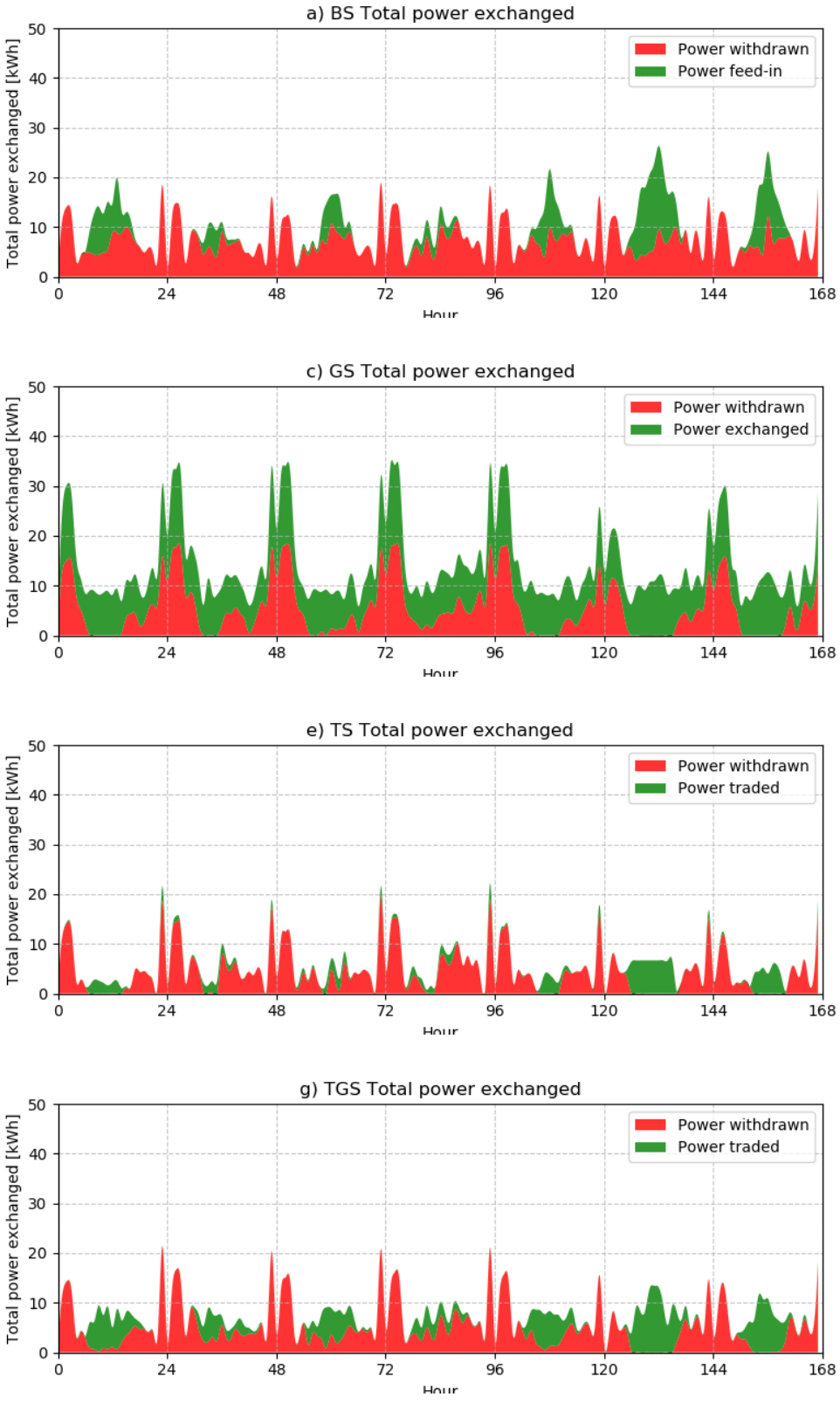

Figure 17: Power exchanged for summer scenarios

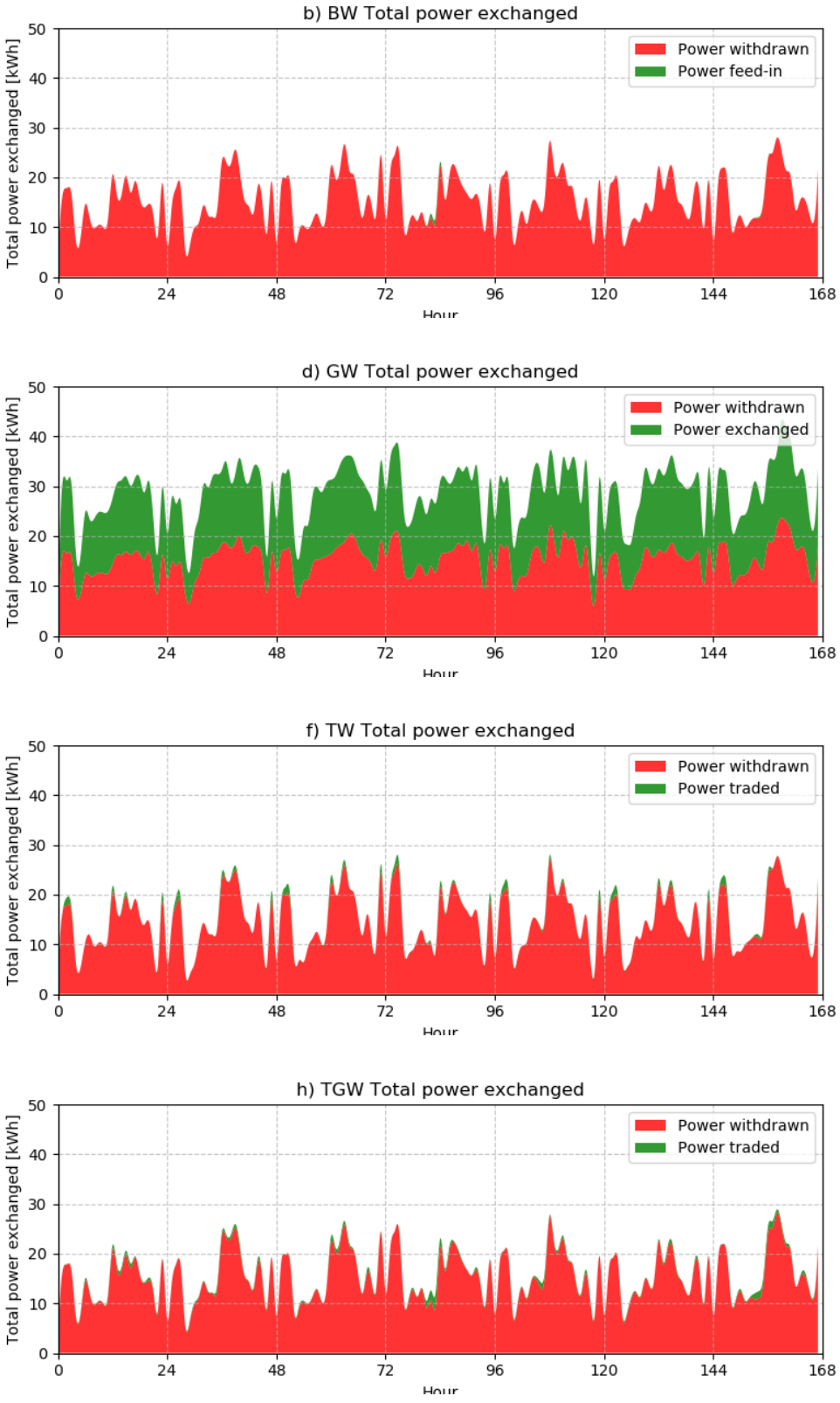

Figure 18: Power exchanged for winter scenarios